

1 **Developing luminescence analysis of Icelandic volcanic glass: a case study**
2 **using the Þórsmörk Ignimbrite**

3

4 Stephen J. Roberts^{1, *}, David C.W. Sanderson², Andrew J. Dugmore³

5

6 ¹ British Antarctic Survey (BAS), Natural Environment Research Council (NERC), High Cross,
7 Madingley Rd, Cambridge, CB3 0ET, UK.

8 ² SUERC, Scottish Enterprise Technology Park, Rankine Avenue, East Kilbride, Glasgow G75
9 OQF, Scotland.

10 ³ School of GeoSciences, University of Edinburgh, Drummond Street, Edinburgh EH8 9XP.

11

12 ***Corresponding author:**

13 e-mail: sjro@bas.ac.uk, Tel: +44 (0)1223 221 339; Twitter: @roberts_sjr

14

15 This manuscript is a preprint, submitted to PLoS One for publication. It has been revised after
16 review and is not yet accepted for publication. Subsequent versions of this manuscript may
17 differ following resubmission and due to the editorial process. If accepted for publication, the
18 final version will be available via the peer-reviewed publication DOI link on EarthArXiv. We
19 welcome any feedback - please send this to the Steve Roberts using the email address above.

20

21

22 **Abstract**

23 Large volcanic eruptions from Iceland can produce significant volumes of glass-rich rhyolitic
24 tephra, which are then deposited across NW Europe and the North Atlantic-Arctic region,
25 forming time-parallel marker horizons useful to palaeoenvironmental studies. Here we
26 investigate new ways of improving the tephrochronological record of Iceland using
27 (thermo)luminescence analysis of rhyolitic volcanic glass shards that dominate airfall ash
28 deposits of the Þórsmörk Ignimbrite (ÞIG), tephra from the Askja 1875 AD, Öræfi 1362 AD
29 eruptions, and the Óþoli tephra from NW Iceland. Following screening experiments, which
30 showed that pure volcanic glass samples retained age-related TL signals, we undertook glass-
31 phase TL dating of the ÞIG and Óþoli tephra. Our TL age estimate of $c. 40 \pm 10$ ka for the ÞIG
32 supports phenocryst-based radiometric ages of $c. 50$ ka rather than older age estimates of $c.$
33 200 ka. Results from the Óþoli tephra were consistent with the fission track age established
34 at $c. 2$ Ma age, but further investigations of high dose sensitivity changes and longer-term
35 stability factors such as athermal fading are required for quantitative dating of volcanic glass
36 deposits >100 ka. However, as thermoluminescence signals from purified glass fractions of
37 Icelandic tephra can be obtained over 100–1,000,000-year time scales, luminescence
38 characterisation of glass shards can be used alongside geochemical and morphological
39 analysis to distinguish between distal tephras with similar geochemical signatures, and assist
40 with tephrochronological investigations beyond the limits of radiocarbon dating.

41

42 **Keywords:** Tephra; geochronology; geochemistry; Arctic; palaeoclimate

43

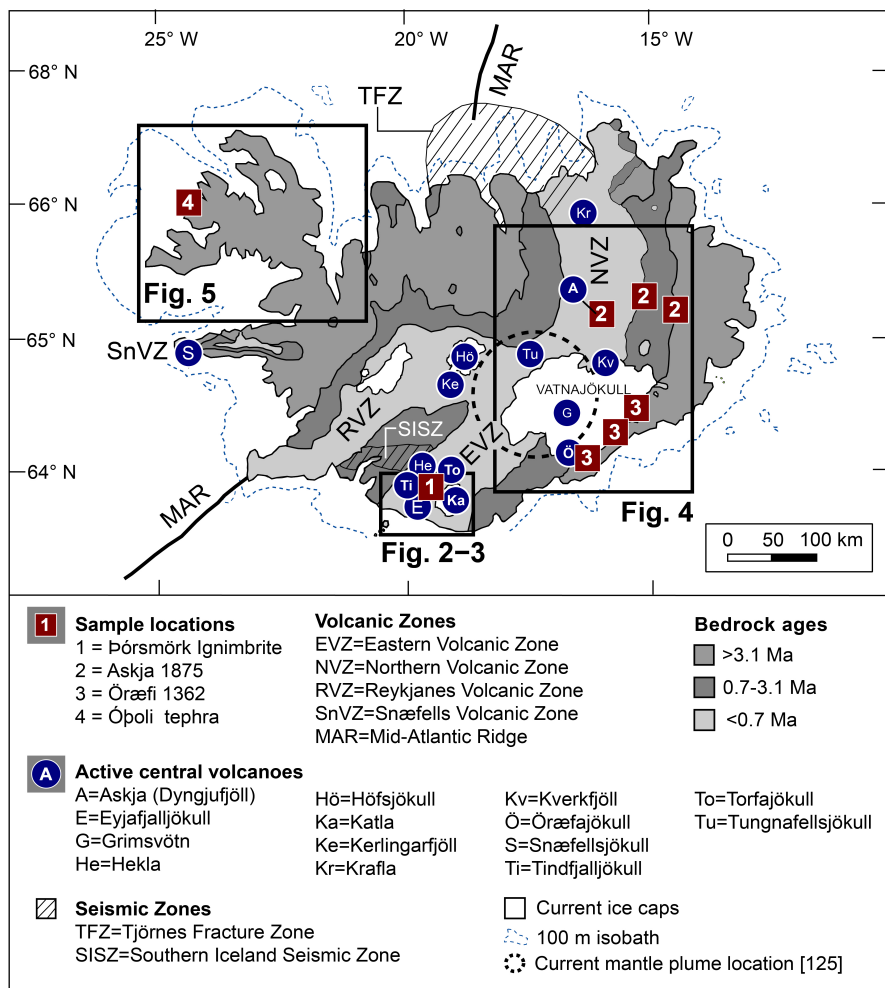
44 **Introduction**

45 Large explosive rhyolite-producing eruptions from Iceland, such as the one responsible for
46 the Þórsmörk Ignimbrite (PIG) in southern Iceland (Fig. 1), are comparatively rare, but
47 particularly useful as they form time-parallel marker horizon, which provide chronological
48 constraints for palaeoenvironmental records. As recent eruptions from Iceland have shown,
49 volcanic ash from even comparatively small eruptions can be distributed across the North
50 Atlantic and Arctic regions, and north-western Europe. Numerous studies have used of tephra
51 layers to link ice, marine and terrestrial records of past environmental and climate change
52 [1–30], but glacial erosion has removed many of the largest eruptions of the pre-Holocene,
53 Quaternary era (>11.7 ka–2.5 Ma) from the Icelandic terrestrial record and some key large
54 Pleistocene eruptions remain relatively poorly characterised and dated near their sources.

55

56 To be useful as time-parallel marker horizons, tephra deposits need to be fully characterised.
57 Major and trace element geochemistry and phenocrystic composition are commonly used
58 alongside shard morphology, texture and chronological data to distinguish between different
59 tephra deposits, and correlate those that are similar [24, 27–42]. However, geochemical
60 correlation based on glass major element geochemistry can sometimes be problematic.
61 Multiple eruptions from the same magma body can produce geochemical heterogeneity
62 within the glassy products of individual deposits [43, 44], but different eruptions from the
63 same magma chamber over a period of time can also produce glass with broadly similar major
64 element geochemical composition. Recent studies have shown there are significantly more
65 visible and non-visible (crypto-tephra) Icelandic ash deposits in sediment cores extracted
66 from the Arctic Sea and North Atlantic than previously thought, and not all can be
67 distinguished by shard-specific major or trace element analysis [33, 37]. Widely dispersed

68 tephra deposits can also be re-deposited a long time after the eruption event by post eruption
 69 processes such as ice-rafting [45, 46] and several studies have confirmed that glass is not
 70 geochemically stable in all burial environments or able to withstand harsh laboratory
 71 digestion procedures intact [47, 48].



72
 73 **Figure 1.** Summary geological map of Iceland showing active central volcanoes and sample
 74 locations [adapted from 11].

75
 76 More than 300 historical eruptions have been documented or identified by geochemical
 77 analysis of tephra layers in Iceland in the last c. 1,100 years, on average, one every four years
 78 [7, 10, 11, 29, 49-59]. Tephra is the only product of more than 130 of these eruptions, and

79 over 75 % of these have produced a visible tephra layer on the Icelandic mainland [60].
80 However, rhyolitic tephra and large ignimbrite-forming eruptions are relatively uncommon in
81 the Icelandic tephrochronological record [13, 15, 37, 53, 61].

82

83 Since rhyolitic magmas produce the most geochemically evolved and distinctive tephra,
84 geochemical discrimination between different volcanic systems and/or multiple eruption
85 events from the same volcanic system can be achieved. Moreover, large volumes of rhyolitic
86 volcanic glass, which are unequivocally associated with the eruption event, form explosively
87 on contact with water and/or ice during magma-quenching. For example, volcanic glass
88 formed from the rhyolitic magma of the Öræfi 1362 AD eruption is geochemically
89 homogenous and has <1% phenocrystic content [62]. Glass-rich volcanic ash ejected into the
90 stratosphere can be distributed over a wide geographical area, forming long-distance
91 chronological markers [63, 64]. Advantageously, selective removal of heavier phenocrystic
92 components during long-distance stratospheric transport of ash provides a natural glass-
93 purification process.

94

95 Radiation induced thermoluminescence (TL) is a well-established property of crystalline
96 minerals such as quartz and feldspars [65]. Non-crystalline materials including synthetic glass
97 [66,67] and naturally occurring volcanic glass (*e.g.*, obsidian) [68] also exhibit TL, though with
98 lower sensitivities than most crystalline materials. A study of 55 archaeological silicate glass
99 slices [66] showed high temperature TL sensitivities ranging from 10^{-1} to 10^2 photon counts
100 per mg per Gy in 10 degree centigrade bands. By contrast TL sensitivities from quartz samples
101 from diverse lithologies have been reported [111] as ranging from 10^3 - 2×10^4 photon counts

102 per mg per Gy over similar temperature intervals (centred on 380 degrees centigrade), and
103 from feldspars from 10^4 - 10^6 photon counts per mg per Gy.

104

105 Therefore, though volcanic glass is a metastable material [72], luminescence signals from the
106 glass phase of tephra provide a useful additional provenance and, potentially, chronological
107 tool, especially in the c. 50-75 ka age-range, which is difficult to date using other radiometric
108 methods (e.g., fission-track) and when suitable phenocrysts are absent [68–72]. Despite the
109 relatively low signal levels, and variability in signal outputs due to retention of some fine
110 crystalline components, pioneering luminescence studies from the early 1980s on fine-
111 grained volcanic glass-rich fractions from tephra deposits from North America and New
112 Zealand showed considerable potential [73–74].

113

114 Here, first, we investigate new ways of improving the tephrochronological record of Iceland
115 by characterising the geochemical and TL properties of the (airfall) rhyolitic glass component
116 that dominates tephra (>95%) from four key rhyolitic Icelandic eruptions of Late Quaternary
117 age: the Þórs mörk Ignimbrite (ÞIG), the Óþoli tephra (ÓT), the Askja 1875 AD (A1875) and
118 Öraefi 1362 AD (Ö1362) eruptions and (Figs. 1–6; Fig. S2, Table S1). Second, we focus on
119 producing quantitative ages from the ÞIG and compare our results to published age estimates.

120

121 Based on geochemical correlation to potassium-argon dated phenocrysts from ignimbrite
122 deposits outside of the Þórs mörk area [1, 2], the ÞIG was originally considered to be c. 200
123 ka. An argon-argon (Ar-Ar) age of 54.5 ± 2 ka [3] has been geochemically linked to the c. 55 ka
124 North Atlantic Ash Zone-II (NAAZ-II) II-RHY-II deposit, a widespread and geochemically
125 homogenous tephra deposit found in North Atlantic and Arctic Sea marine sediment cores

126 Greenland ice core records [3–5]. The eruption that formed the ÞIG is the same order of
127 magnitude as the thickest rhyolitic tephra layers in the Holocene and historical
128 tephrochronological record of Iceland, *e.g.*, Hekla 3, Hekla 4, Öræfi 1362 AD and Askja 1875
129 AD [11, 76, 88, 89].

130

131 The Óþoli tephra was found in plateau-top ice-dammed lake deposits of NW Iceland.
132 Following initial TL analysis which suggested an early Quaternary age and has been fission-
133 track dated to 2.26 ± 0.11 Ma [75]. In this study, the tephra deposit acts as an ‘older’ age-
134 comparison for quantitative TL dating of purified volcanic glass from the ÞIG.

135

136 The A1875 and Ö1362 tephra deposits examined are from two of the largest rhyolite forming
137 Plinian-style eruptions in the Icelandic historical record. These eruptions distributed large
138 volumes of tephra across eastern Iceland and NW Europe. In this study, we use them as
139 ‘recent’ TL age-controls because they have similar glass-phase rhyolitic geochemistry to the
140 Óþoli tephra and the ÞIG.

141

142 **Study sites**

143

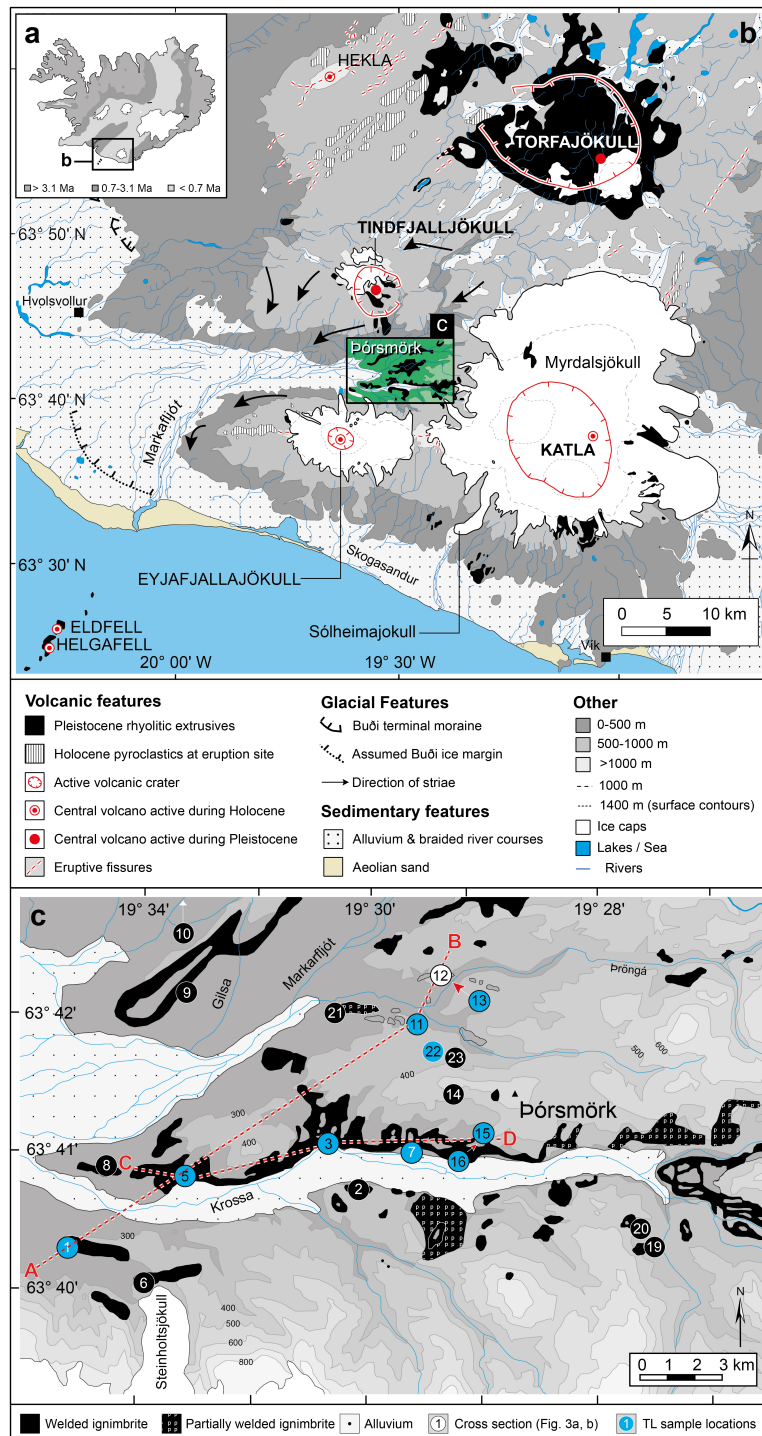
144 **Þórsmörk Ignimbrite:** The Þórsmörk Ignimbrite (ÞIG), first described by Thórarinsson [1] and
145 named by Jørgensen [76, 77], is located in the transitional-alkalic province of the Eastern
146 Volcanic Zone (Fig. 1). It is one of Iceland’s largest eruptive bodies, covering an area of about
147 80 km² (Figs. 2, 3). Outcrops in the Þórsmörk area are the only known record of the ÞIG-
148 forming eruption in the Icelandic terrestrial tephra record. Intermittent volcanic aggradation
149 and glacial erosion have exposed well-preserved stratigraphic sections along the Krossa and

150 Markarfljót valleys, with deposits north of the Krossa that are typically 10–50 m thick but can
151 be up to 200 m thick [76, 77] (Figs. 2, 3). Accessible exposures, up to 30 m thick, are located
152 on a 4–5 km stretch along the northern border of the Krossa (Figs. 2, 3). No basal contact is
153 visible at most sites and only slope deposits are accessible at some sites [1, 76] (Fig. 3).

154

155 The Þórsmörk area is surrounded by three ice-capped, active central volcanoes:
156 Eyjafjallajökull to the south, Katla to the east, Tindfjalljökull to the north (Fig. 2b). Torfajökull,
157 Iceland's largest active rhyolite volcano, is located further to the NE and Hekla is located
158 further north beyond Tindfjalljökull. Torfajökull is amongst the most active rhyolitic volcanoes
159 in the world with at least ten rhyolitic eruptions in the post-glacial period alone with the last
160 occurring in ca. 1480 AD [78]. Tindfjalljökull is the least active central volcano in this region
161 and classified as a dormant volcano because there have only been a few eruptions along its
162 margins in post-glacial times [1, 79, 80]. Eruptions from Tindfjalljökull are typically dominated
163 by slightly alkaline basalts and minor intermediate rocks and abundant sub-alkaline to slightly
164 peralkaline rhyolites [76, 80–83]. Thórarinsson suggested that the summit of Tindfjalljökull is
165 collapse caldera connected with the formation of the ÞIG [1, 76, 84]. All structural and
166 depositional features of the ÞIG preserved in and around Þórsmörk are associated with
167 emplacement from pyroclastic flows or surges [76, 77] (Fig. 3). Jørgensen [76, 77] found no
168 evidence for a Plinian phase of activity, but abundant airfall ash deposits (*e.g.*, Fig. 3i–l) could
169 have been formed by explosively-generated pyroclastic flows, created by instabilities in the
170 lower parts of the eruption column [85]. These combined into an ignimbrite-forming surge
171 that mantled the existing topography, with welded and unwelded pumice and ash forced into
172 valley troughs and sides. Given an average thickness of 20–25 m, Thórarinsson [1] calculated
173 that the equivalent volume of the ÞIG as 1.5–2.0 km³. At least a further 2–3 km³ of freshly

174 fallen tephra was probably dispersed over a wider area, but this has since been eroded by
 175 glacial activity.

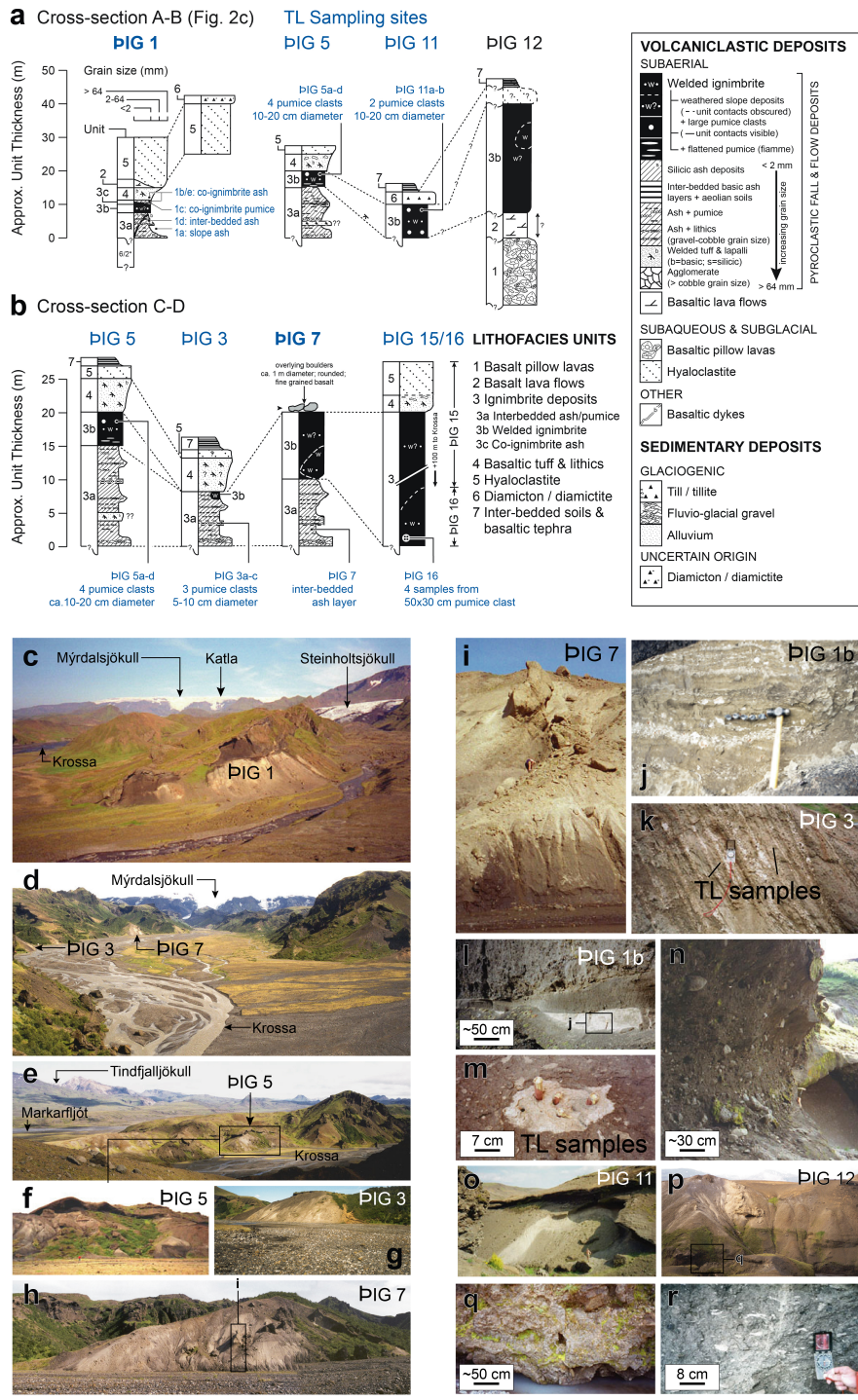


176
 177 **Figure 2. Regional setting and sampling locations for the Þórsmörk Ignimbrite. (a)** Location
 178 map of Iceland; **(b)** Location map of Þórsmörk in relation to active volcanoes, pyroclastic and
 179 extrusive deposits and main glacial features of the Eastern Volcanic Zone (EVZ), Iceland. The

180 geology of area covered by the Þórsmörk box is basic and intermediate hyaloclastites and
181 tuffaceous sediment younger than 0.7 Ma (based on the 1:250,000 Geological Map no. 6 of
182 the Iceland Geodetic Survey). **(c)** Sketch map of main outcrops of the Þórsmörk Ignimbrite,
183 and its broad classification into welded and unwelded outcrops [adapted from 76, 77] and
184 thermoluminescence sampling locations (blue circles) investigated in this study. Some sample
185 sites (*e.g.*, ÞIG10) were located off-map, while others (*e.g.*, ÞIG12) were inaccessible.

186

187 Thórarinsson [1] and Jørgensen [77] suggested a c. 200 ka age for the ÞIG by correlating
188 deposits in Þórsmörk with potassium-argon (K-Ar) ages from geochemically similar deposits
189 north of Þórsmörk [2, 4]. Zielinski et al. [9] later proposed that the ÞIG was the source of the
190 rhyolitic component of North Atlantic Ash Zone-II (NAAZ-II), a widespread tephra deposit that
191 has been found in numerous marine and ice cores across the North Atlantic and the Arctic
192 Sea (Fig. S2). Dated to c. 50 ka, based on its correlation-based age in the GISP2 Greenland ice
193 core of 53.5-55 ka [9, 86, 87], NAAZII has been geochemically linked with an argon-argon (Ar-
194 Ar) dated ÞIG deposit of 54.5 ± 2.0 ka, sampled from an unspecified location [3].



195

196 **Figure 3. The Þórsmörk Ignimbrite, southern Iceland. (a–b)** Summary composite schematic
 197 stratigraphic logs of main lithofacies units at principal sites and schematic cross section
 198 sketches along lines A-B and C-D; **(c–r)** Photographs of the Þórsmörk Ignimbrite sampling
 199 locations and luminescence sampling methods: **(c)** Site PIG 1, taken from the lateral moraine
 200 of Gigjökull, looking approximately E up the Krossa towards Mýrdalsjökull; **(d)** Sites PIG 3 & 7,

201 taken from Valahnjúkur looking approximately E up the Krossa towards Mýrdalsjökull; **(e)** Site
202 PIG 5, taken from the top of site PIG 6, looking approximately NNE towards Tindfjalljökull in
203 the distance; **(f)** Site PIG 5; **(g)** Site PIG 3 looking approximately W down the Krossa; **(h)** Site
204 PIG 7 taken from the Krossa sandur looking N at sampling site, and erratics near the top of
205 the deposit (circled); **(i)** TL sampling at site PIG 7 composed of inter-bedded ash, pumice and
206 lithic layers beneath an outcrop of welded ignimbrite, similar to those at PIG 3, shown in (k);
207 **(j)** TL sampling at PIG 1b in ash rich co-ignimbrite ash and pumice layers; **(k)** TL sampling of
208 inter-bedded ash layers at PIG 3; **(l)** Co-ignimbrite ash, black tuff and capping hyaloclastites
209 at site PIG 1b (Units 3c, 4, 5); **(m)** TL sampling of a large pumice clast, c. 25–30 cm in diameter,
210 embedded in a welded ash and lithic matrix at site PIG 16; **(n)** Poorly sorted, rounded boulders
211 and pebbles in loose soil and fine-grained matrix (diamicton) contact with welded ignimbrite
212 at site PIG 11 (hammer for scale); **(o)** Site PIG 11 looking NNE (person at the bottom edge of
213 the shadow for scale); **(p)** Site PIG 12 taken from the top of the hill at site PIG 13 looking
214 approximately north; **(q)** Pillow lavas at the base of PIG 12; **(r)** Fiamme at the base of PIG 5
215 (Unit 3b).

216

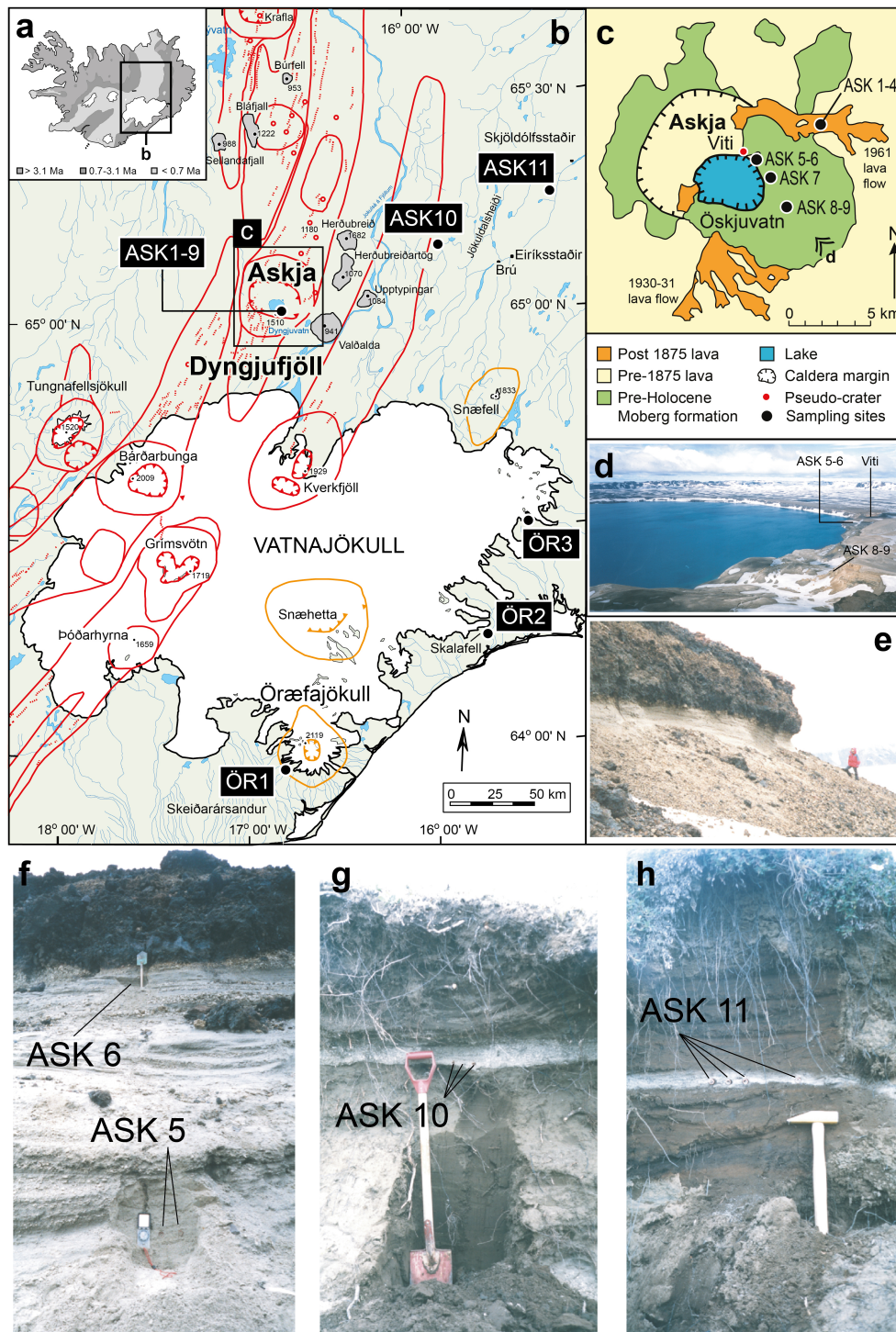
217 **Askja 1875 AD (A1875) tephra:** Post-glacial volcanism in Iceland is concentrated in four
218 separate areas within the fissure system of Dyngjufjöll (Askja), located approximately 100 km
219 North of Vatnajökull in the Eastern Highlands of the tholeiitic Northern Volcanic Zone (NVZ)
220 of Iceland (Figs. 1, 4) [83]. Askja, the name of the main caldera and central volcano, covers an
221 area of c. 45 km² (Fig. 4) and is bounded by steep cliffs, with Pleistocene-age rocks and
222 predominantly basaltic composition forming the basement bedrock inside the crater (Fig. 4)
223 [89]. Post-glacial lavas contain several rhyolitic ash layers, the oldest dated to c. 9,800 years
224 BP [90]. Between 9,800-4,500 years BP, following rapid early Holocene deglaciation in Iceland,

225 volcanic productivity was 30 times greater than during the historical era [90]. The last Plinian
226 eruption in the Dyngjufjöll volcano took place from within the Askja caldera a few hours
227 before 8 a.m. on 29th March 1875 AD [90, 91]. The explosive phase of the eruption produced
228 large volumes of fine-grained, grey-white, non-vesicular ash, which was dispersed across
229 eastern Iceland by strong westerly winds forming visible layers 20-30 cm thick up to 50 km
230 away [6]. The A1875 eruption is a classic example of how tephra from explosive Icelandic
231 eruptions can be rapidly distributed across the North Atlantic and NW Europe [92, 93]. Tephra
232 layers dominated by glass-shards invisible to the naked eye with a similar eruption-related
233 geochemistry to A1875 deposits in Iceland have been found in Scandinavia [90, 94].

234

235 **Öræfi AD1362:** The Öræfajökull volcano, located in the Eastern Volcanic Zone on the southern
236 margins of the Vatnajökull ice cap (Figs. 1, 4b), is Iceland's highest (2119 m) and most active
237 composite stratovolcano during the post-glacial and Holocene era. There have only been two
238 rhyolite-producing eruptions from Öræfajökull in the historical period: in 1362 AD and 1727
239 AD [11]. The 1362 AD eruption (henceforth referred to as Ö1362) was particularly explosive,
240 producing >10 km³ of freshly fallen rhyolitic ash and pumice, and accompanied by two massive
241 jökulhlaups from Falljökull and Rótarfjallsjökull. Although the eruption took place mainly in
242 the caldera, and most of the fallout occurred over the sea, it is still the second most
243 voluminous tephra deposit in Iceland in recorded history, after the more effusive and basaltic
244 tephra producing Veiðivötn eruption of 1477 AD [58]. Up to 2 km³ of highly evolved rhyolitic
245 (SiO₂>70%) tephra fell on land with prevailing westerly winds transporting most of the ejecta
246 ESE across the North Atlantic [11, 62, 95]. Tephra layers up to 10 cm thick have been found in
247 soils covering an area of 4300 km² surrounding the main edifice [96].

248



249

250 **Figure 4. Historical eruption age-control study sites and sampling of A1875 and Ö1362**

251 **tephra deposits. (a)** Location map; **(b)** Regional setting of the Askja (Dyngjufjöll) (red) and the

252 Öraefi (orange) volcanic systems and Askja 1875 (ASK1-11) and Öraefi 1362 (ÖR1-3) sampling

253 locations. Solid red & orange lines are outlines of the main volcanic systems; broken lines red

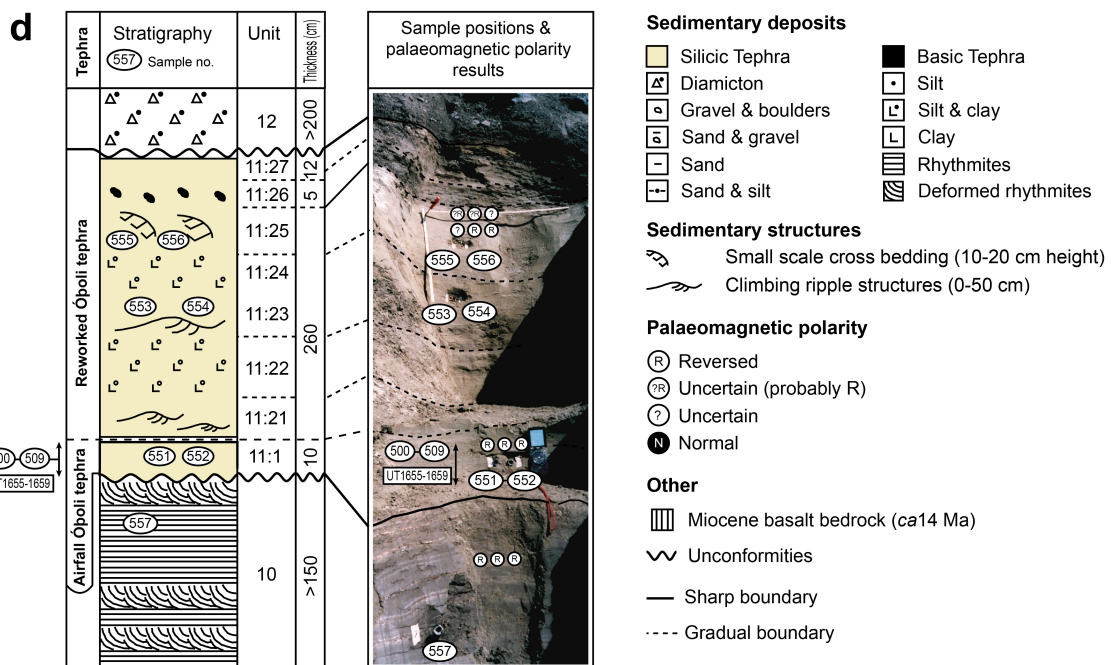
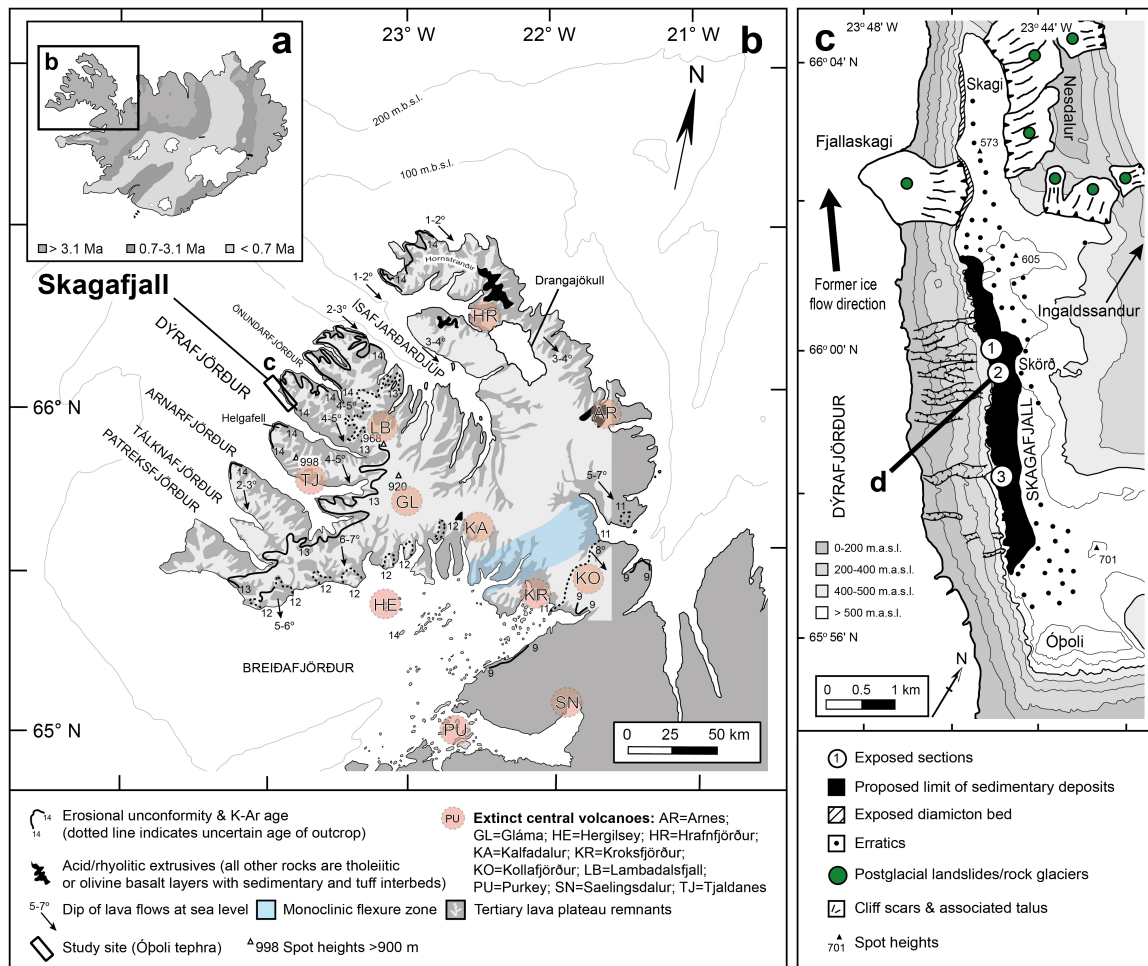
254 and orange lines are fissure swarms; triangulated lines are the caldera margin; red circles are

255 craters and grey areas outlines of the main table mountains ('mobergs'). **(c)** Summary
256 geological map of Askja adapted from [89] and showing the location of samples ASK 1-9. **(d)**
257 Askja caldera from SE rim and ASK 5-9 sampling sites; **(e)** A1875, Layer 'D' [89] and capping
258 lava flow; **(f)** TL sampling of Askja 1875 - ASK 5 (Layer 'C' [89] and ASK 6 (Layer 'D' [89]); **(g)**
259 ASK 10 at Fiskidalur, 55 km NNE of Askja; **(h)** ASK 11 at Arnórsstaðamuli, 74 km NNE of Askja.
260

261 **Óþoli Tephra:** The Óþoli tephra (ÓT) is a rhyolitic tephra deposit within a glacio-lacustrine
262 sedimentary sequence near the plateau surface of Skagafjall [75, 97] (Fig. 5a–c). The ÓT
263 sedimentary unit consists of 8-10 cm of airfall tephra overlain by up to c. 10 m of reworked
264 volcanic ash (Fig. 5d). The airfall ash sub-unit is composed of more than 99% rhyolitic glass,
265 with very minor basaltic–andesite/andesitic altered glass and sparse traces of feldspar, iron
266 ore and pyroxene of uncertain origin [75, 97]. The 8–10 cm thick airfall ash is unusual for a
267 tephra deposit on the NW (Vestfirðir) Peninsula, where visible tephra layers in Holocene peat
268 deposits are uncommon, and usually less than a centimetre thick (Fig. 5d). Based on its
269 stratigraphic position within an ice-dammed lake sequence in NW Iceland, the ÓT was
270 originally thought to have been deposited c. 17–23 ka [97], but has since been dated to 2.26
271 ± 0.11 Ma using the isothermal fission-track method [75]. Prior to fission-track dating analysis,
272 preliminary luminescence experiments on the airfall rhyolitic glass fraction revealed the ÓT
273 to be older, with a minimum age estimate of at least c. 400 ka (Fig. 6f) [75]. The ÓT is most
274 likely the product of a large Plinian-style eruption somewhere in the Húsafell region, a now
275 inactive part of the SW Iceland axial rift (RVZ in Fig. 1) from near-central Iceland [75].
276 Prevailing north/north-north-westerly winds at the time of the eruption transported ash c.
277 200 km, depositing it on the heavily glaciated landscape of the Vestfirðir Peninsula during the

278 Late Pliocene [75]. The A1875 tephra is the closest geochemical match to the Ópoli tephra

279 (Figs. 1, S1) [75].



280

281 **Figure 5. Regional setting, stratigraphic logs and sampling of the Óþoli tephra. (a–c)** Location
282 of Skagafjall and main geological features of the Western Troughs of the Vestfirðir Peninsula
283 (based on [75, 97]). **(d)** Detailed stratigraphic log of and summary of palaeomagnetic results
284 from Skagafjall section B units 10–12 and sampling strategy/sample numbers for the air fall
285 and reworked components of the Óþoli tephra. Sample numbers 500-510 and 551-557 are
286 SUTL laboratory numbers (SUERC-luminescence dating laboratory) sampled from the airfall
287 tephra deposits in section B. SUTL558 is from section C. SUTL500-509 were sampled at 1 cm
288 intervals from the basal 10 cm of Óþoli tephra above the rhythmite bed/tephra contact; UT
289 sample numbers are University of Toronto fission-track laboratory numbers [97].

290

291 **Methods**

292 Luminescence dating relies on the laboratory reconstruction of the radiation dose absorbed
293 by sensitive materials in the natural environment since formation or since the last heat- or
294 light- induced resetting or ‘zeroing’ event [98–100]. For volcanic glass, the event being dated
295 is the formation event, *i.e.*, cooling from magma, which due to its extremely high
296 temperature, may be assumed to be free from residual thermoluminescence signals. Here,
297 this assumption was verified, for practical purposes, using 19th Century material from the
298 A1875 eruption. A laboratory determination of the total radiation dose experienced since the
299 formation or last bleaching event is referred to as the equivalent or palaeodose, D_e . This is
300 obtained, following measurement of the “natural” luminescence signal in the laboratory by
301 reconstructing a stepwise luminescence dose-response curve by laboratory irradiation, and
302 remeasurement of stimulated luminescence from purified sub-samples (or aliquot discs). If
303 D_T , the rate of radiation dose received by decay of radioactive elements, and cosmic
304 radiation, *in-situ* in the natural environment, can be reliably assessed [99, 100], an age

305 estimate can be determined, simply, as the quotient of palaeodose (D_e) and environmental
306 dose rate (D_T) or $[D_e / D_T]$.

307

308 ***Sample collection and purification***

309 We examined the luminescence characteristics of undisturbed airfall deposits to avoid
310 possible complications associated with post-depositional reworking and light exposure.

311 Samples were collected by hammering light tight 22–27 mm diameter, 20–50 cm long copper
312 tubes into airfall tephra and pumice deposits that had been cut back 10–30 cm. All samples
313 were transported and stored under light-tight conditions and 2–5 cm of material at the end
314 of the tubes that could have been exposed to light was removed.

315

316 Contaminant mineral phases that also retain a luminescence signal, such as quartz, feldspar
317 and zircon, have a higher density ($>2.45 \text{ g cm}^{-3}$) than rhyolitic glass ($2\text{--}2.2 \text{ g cm}^{-3}$). Therefore,
318 double-purified sieved 90–150 μm volcanic glass fractions were prepared by density
319 separation techniques [48, 73, 102]. Samples were cleaned ultrasonically in 10% hydrochloric
320 acid (HCl) and density separated 2.3–2.4 or $<2.4 \text{ g cm}^{-3}$ using sodium polytungstate solution
321 (Figs. S3). Harsh chemical treatments and etching were avoided due to the fragile nature of
322 platey and pumiceous glass shards; hence, no attempt was made to clean the glass surfaces
323 with hydrogen peroxide (H_2O_2) or etch the shards with hydrofluoric acid (HF) to remove their
324 thin outer layer influenced by external alpha-dose rates. Contamination by non-glassy phases
325 was assessed using TL sensitivity response, and visually confirmed by light microscopy and
326 Scanning Energy Dispersive-Scanning SEM (EDS-SEM) geochemical mapping of discs used in
327 TL analysis and by examination of preliminary N/50 Gy dose response curves (Fig. 6, S4). A
328 summary

329

330 ***SAR-TL experiment***

331 Based on findings from our preliminary screening experiments (Fig. 6), and after testing
332 multiple aliquot methods [101], it was noted that the relatively high radiation doses needed
333 to match natural signals from the early Quaternary Ópoli tephra analysis had potential to
334 induce radiation colouring in the samples. Moreover, sensitivities in response to repeated 50
335 Gy irradiation and readout cycles tended to decline, suggesting that such radiation colouring
336 was not being fully annealed by the TL heating cycle to 400 degrees. In recognition of this, to
337 quantify equivalent doses and constrain ages for the Þórsmörk Ignimbrite and the Ópoli
338 tephra, we adapted the Single-Aliquot Regeneration OSL (SAR-OSL) technique [103, 104] for
339 TL analysis (SAR-TL) . In the SAR method, the same disc is exposed to a series of laboratory
340 radiation doses prior to preheating and readout, followed by a test dose (TD) measurement
341 to assess laboratory induced sensitivity changes across the measurement cycle. The natural
342 TL was measured from purified glass on each disc, and TL was then artificially regenerated
343 beyond the naturally accumulated TL by applying a series of laboratory radiation doses to
344 each disc.

345

346 Stainless steel discs were cleaned with acetone and Electolube SCO200D silicone grease then
347 loaded with 4–6 mg of purified volcanic glass concentrated in the central area of each disc.
348 Read-outs were undertaken using a Scottish Universities Environmental Research Centre
349 (SUERC) TL Research Reader consisting of an Electron Tubes 9883 QB Photo-multiplier Tube
350 (PMT) fitted with Schott 7/59 and KG1 filters and continuously flushed with nitrogen to
351 prevent oxidising reactions that might create spurious TL. Measurements were undertaken
352 manually with real time analysis to monitor glow shapes, assess integrated photon count

353 rates to define successive regeneration doses levels required, and check for signal quality.
354 Discs were heated from room temperature to 400 °C at 5 °C s⁻¹. Blanks and blank
355 contamination discs were cleaned with acetone and sprayed with Electrolube SCO200D
356 silicone grease, were placed on the work surface and read out at the end of each session.
357 Discs for the N/50 Gy and SAR-TL experiment were irradiated using a shielded ELSEC 9022
358 irradiator fitted with a 1.85 GBq ⁹⁰Sr β-ray source with a source to sample distance of 15 mm
359 and a silicate dose rate of 3.353 ± 0.015 Gy min⁻¹ for the N/50 Gy experiment and 3.270 ±
360 0.015 Gy min⁻¹ for the later SAR-TL experiments. Reconstructing the large natural signal
361 retained in the Ópoli tephra proved particularly time consuming due to its large stored natural
362 dose. For this experiment a higher dose rate irradiator incorporating a 11.1 GBq ⁹⁰Sr β-ray
363 source at a working distance of 7.5 mm was used, yielding a mean dose rate in the central
364 areas of the sample of 32.0 ± 0.6 Gy min⁻¹. Both irradiators had been calibrated to high
365 precision relative to the UK air kerma standards at the National Physical Laboratory (NPL)
366 when commissioned in 1997, before this study.

367

368 ***SAR-TL Palaeodose reconstruction (D_e)***

369 After the natural TL signal had been thermally removed and measured (read-out), the TL and
370 test dose and read-out measurement cycle for each disc consisted of: (1) Individual disc
371 irradiation (PIG: 50, 75, 100, 125, 150, 200, 300 Gy; ÓT: 500, 1000, 1500, 2000, 3000, 4000,
372 5000, 6000 Gy); (2) A short, high temperature (within-chamber) pre-heat of 220 °C for two
373 minutes and 0–400 °C TL read-out; (3) Test-dose (TD), pre-heat, as stage 2, and 0–400 °C TL
374 read-out. Disc-specific changes in sensitivity were in stage 3 were corrected by applying a test-
375 dose (TD) after each successive regeneration dose (PIG = 25 Gy; ÓT = 100 Gy). Palaeodose (D_e)
376 values for the Þórsmörk Ignimbrite ÞIG7 and the Ópoli tephra SUTL551 samples were

377 calculated from standard error weighted regression of 200–400 °C, 10 °C integrated data
378 (Tables 1, 2, S2, S4). The final weighted mean palaeodose values used in age estimates were
379 calculated from the most thermally stable peak intensity regions of the glow curve,
380 determined by a D_e plateau plot. In summary, D_e values were integrated over three
381 temperature regions that correspond to the wide (280–360 °C), median (290–330 °C) and
382 narrow (290–310 °C) TL intensity peak region of the glow curves (Figs. 7–8; Tables 1, 2).
383 Uncorrected (UC) and test-dose (sensitivity) corrected (TDC) regeneration curves, were
384 modelled using best mathematical fit (highest adjusted r^2 values, p -value <0.05) linear
385 regression ($y=ax+b$) and non-linear least squares saturating exponential regression analysis
386 ($y=a[1-e^{-bx}]$) applied to 10 °C interval datasets for both samples (Tables S2, S4). The non-
387 linear and non-saturating response of the Ópoli Tephra was also modelled using saturating
388 exponential + linear regression analysis ($y=a[1-e^{-bx}] + cx$) [following 66]. Regression results
389 shown in Tables 1 and 2 represent methods with the highest r^2 and lowest RMSE values (see
390 also Table S2, S4). Other regression models (e.g., saturating exponential, 2nd and 4th order
391 polynomial) were investigated (e.g., Table S4). Regression and statistical analysis was
392 undertaken in SigmaPlot (Systat Software Inc., San Jose California USA,
393 www.systatsoftware.com), XLSTAT (version 2010.3.09, www.xlstat.com).

394

395 Fading tests were conducted at the end of the measurement cycle using multiple aliquot
396 grouped approaches as suggested by Sanderson 1988 [116]. For this, two groups of discs were
397 defined for each sample. As these had same prior radiation and TL readout histories as each
398 other, both groups were expected to be in the same state, in respect of sensitivity and
399 sensitisation behaviour. One of the groups was irradiated to a 50 Gy dose, at the start of the
400 test period, and the other irradiated at the end of it – 5×10^6 seconds. Both were preheated

401 together, and then readout, in their 9th readout cycle since the start of the experiment. These
402 results were normalised to those obtained from a prompt readout in their 8th cycle. By double
403 normalising the data sets and comparing the results from the two groups, the fading quotient
404 associated with the dark storage for the period between prompt and stored readings was
405 obtained. This approach provides for replication across many discs, and importantly is not
406 affected by sensitivity changes in the samples (based on sensitisation between successive
407 irradiation and readout cycles), or in the equipment (since the readout sessions for both
408 groups of samples are conducted together both for the prompt and stored measurements).
409 The fading observed crosses log time cycles 4-5 and 6-7.

410

411 A similar approach was adopted by Ward [67], who studied TL dose response, from 200 Gy to
412 160 kGy, and stability of highly reproducible mass produced and fully melted silicate glass
413 slices (i.e., microscope cover slips). Fading tests using high dose (44 kGy) covered 11
414 logarithmically spaced post-irradiation intervals from 45 minutes after irradiation up to 35
415 days. After an initial rapid fading over the first few hours following irradiation, subsequent
416 losses diminished in rate as seen on a logarithmic time scale and appeared to be dominated
417 by thermal fading processes. On this basis, the procedure adopted in the study aimed to avoid
418 the immediate post-irradiation period. It is recognised that fading rates over longer
419 Quaternary timescales represent an extrapolation over any observable laboratory storage
420 test. Therefore, the results of the study were also be assessed relative to independent age
421 controls of the Ópoli tephra and PIG in this study.

422

423 ***Dose rate reconstruction (D_T)***

424 The overall dose rate to the tephra shards includes internally generated alpha and beta
425 contributions, and externally delivered alpha, beta, gamma components from the bulk
426 sediment matrix, which are attenuated by water, plus an external cosmic dose rate
427 component (Tables 3, 4). Bulk sample geochemical data, obtained by X-ray fluorescence (XRF)
428 and Inductively Coupled Plasma-Mass Spectrometry (ICP-MS) analysis, was used to assess
429 'external' or 'bulk' matrix dose-rates. Bulk dose rate calculations were based on the infinite
430 matrix assumption [100], which states that samples are essentially homogeneous on a
431 macroscale. Shard-specific electron probe microanalysis (EPMA) potassium (K) data and ICP-
432 MS analysis of the purified glass fraction U, Th and Rb data were used for (internal) glass-
433 shard dose rate calculations, ($D_T^{\text{shard}}(\text{in-situ-sat})$) in Table 4, following [98, 100]. See
434 Supplementary Note 1 for experimental procedures. We also compared dose rates derived
435 from bulk and glass shard geochemistry with data derived from spectrometry measurements
436 (Tables 3, 4, S5).

437

438 For the most realistic assessment of dose rate, we partitioned the shard alpha dose into an
439 internal contribution, which is not subject to water-content attenuation, and an external
440 alpha contribution, delivered across the pore space of the bulk matrix, which is attenuated by
441 pore-water. For the final weighted mean glass-bulk dose rate model, $D_T^{\text{glass-bulk}}(\text{in-situ-sat})$ (Table
442 4), we partitioned the dose rate into internal glass shard and external matrix components
443 according to water content attenuation as follows. Samples for this study were collected
444 during the warmest and driest parts of the year. Since the Icelandic climate is significantly
445 colder and wetter outside our sampling months of June-August, we defined the mean water
446 content as the mid-point of the collected and saturated water content and applied a 15%
447 error to cover possible fluctuations in water content during burial [following 105].

448

449 Dry dose rates were attenuated by appropriate factors before calculation of final 'wet' dose
450 rates using equations in [100], as follows: α -wet = α -dry / (1 + 1.5WF); β -wet = β -dry / (1 +
451 1.25WF); γ -wet = γ -dry / (1 + 1.14WF), where W and F are as defined W = (saturation wet
452 weight - dry weight) / (dry weight). F = average fractional water content during burial history
453 and was determined for two scenarios: as received water content (*in-situ*) and average
454 palaeowater content, i.e., the mid-point between *in-situ* and saturated water content, with
455 error limits that encompass the measured $F_{in-situ}$ and $W_{saturation}$ values. Errors in $F_{in-situ}$ are mean
456 $\pm 1\sigma$ of three representative measurements, while $W_{saturation}$ errors are measurement errors
457 from six duplicate measurements.

458

459 Internal (glass) and external (bulk) dose rates were based on geochemical and/or
460 spectrometry data according to the following equations: $D\alpha_T = k[\phi_g D\alpha_g + (1-\phi_M)WFD\alpha_M]$ and
461 $D\beta_T = \phi_g D\beta + (1-\phi_M)WFD\beta_M]$, where: ϕ_g , ϕ_M are published absorbed dose factors and (1- ϕ_M)
462 attenuation factors [107–109] that correspond to the median grain size for glass shards and
463 matrix, respectively. Spectrometry-based dose rates were calculated from *in-situ* portable
464 gamma-spectrometry, thick source beta counting (TSBC) and alpha spectrometry (Table 4).
465 Geochemical-based dose rates were calculated from bulk and shard-specific geochemical
466 data in Tables 4 and S1 using well-established conversion factors [109]. No thoron or radon
467 loss was assumed in conversion calculations because samples are believed to be sufficiently
468 compact. External attenuation factors for U, Th and K taken from [108] were based on a
469 median grain-size of 100 μm . Equilibrium between U and Th decay was assumed as similarities
470 between elemental and TSBC dose rates suggested that disequilibrium between decay
471 products is minimal.

472

473 **Results**

474 ***Sample collection, purification & preliminary dose response screening***

475 We collected light-tight TL samples from 17 out of 23 locations visited in the Þórsmörk region
476 (Figs. 2, 3). Samples covered a wide range of rhyolitic material, including pumice, airfall ash
477 layers dominated by glass shards, inter-bedded rhyolitic ash layers associated with pyroclastic
478 flow deposits, and reworked ash deposits overlying the pumice-rich horizons (Fig. 3; Table
479 S1). Sampled pumice clasts were unwelded and typically c. 10–50 cm in diameter (Fig. 3m).
480 Ten light-tight samples were collected from airfall and reworked Óþoli tephra deposits (Fig.
481 5). Light-tight samples of A1875 tephra were collected from three locations: 0.5 km SE of Víti
482 within the caldera (ASK 5) (ash-rich layers C & D [90]), 55 km to the ENE of Víti at Fiskidalur
483 (ASK 10), and 74 km NNE of Víti at Arnórsstaðamuli (ASK 11), where visible layers, up to 1 cm
484 thick exist (Fig. 4). Ö1362 tephra samples were collected from three sites at 9 km (Kvísker),
485 65 km (Hólmur), 86 km (Fóssdalur) to the East of the volcano along the principal eruption
486 plume axis (Fig. 4). The major element geochemical composition of the rhyolitic glass-shards
487 in the Ö1362 tephra is most similar to those of the Þórsmörk Ignimbrite (Fig. S2).

488

489 Visual inspection under the microscope revealed the rhyolitic ash and pumice Þórsmörk
490 Ignimbrite samples were >95% glass, and the Óþoli tephra samples were >99% clear, platy
491 glass shards of rhyolitic composition (Fig. 6). The bulk A1875 and Ö1362 samples were
492 composed of >90–95% platy or pumiceous volcanic glass shards (Fig. 6). Þórsmörk Ignimbrite
493 samples had the highest glass-shard alkali (Na+K) content of samples examined (Fig. S2). No
494 purified fractions or SEM-EDS geochemical maps of discs used in SAR-TL experiments had

495 exceptionally high K, Na, Ca, indicative of possible feldspar contamination (K, Na, Ca)AlSi₃O₈,)
496 (Fig. S5).

497

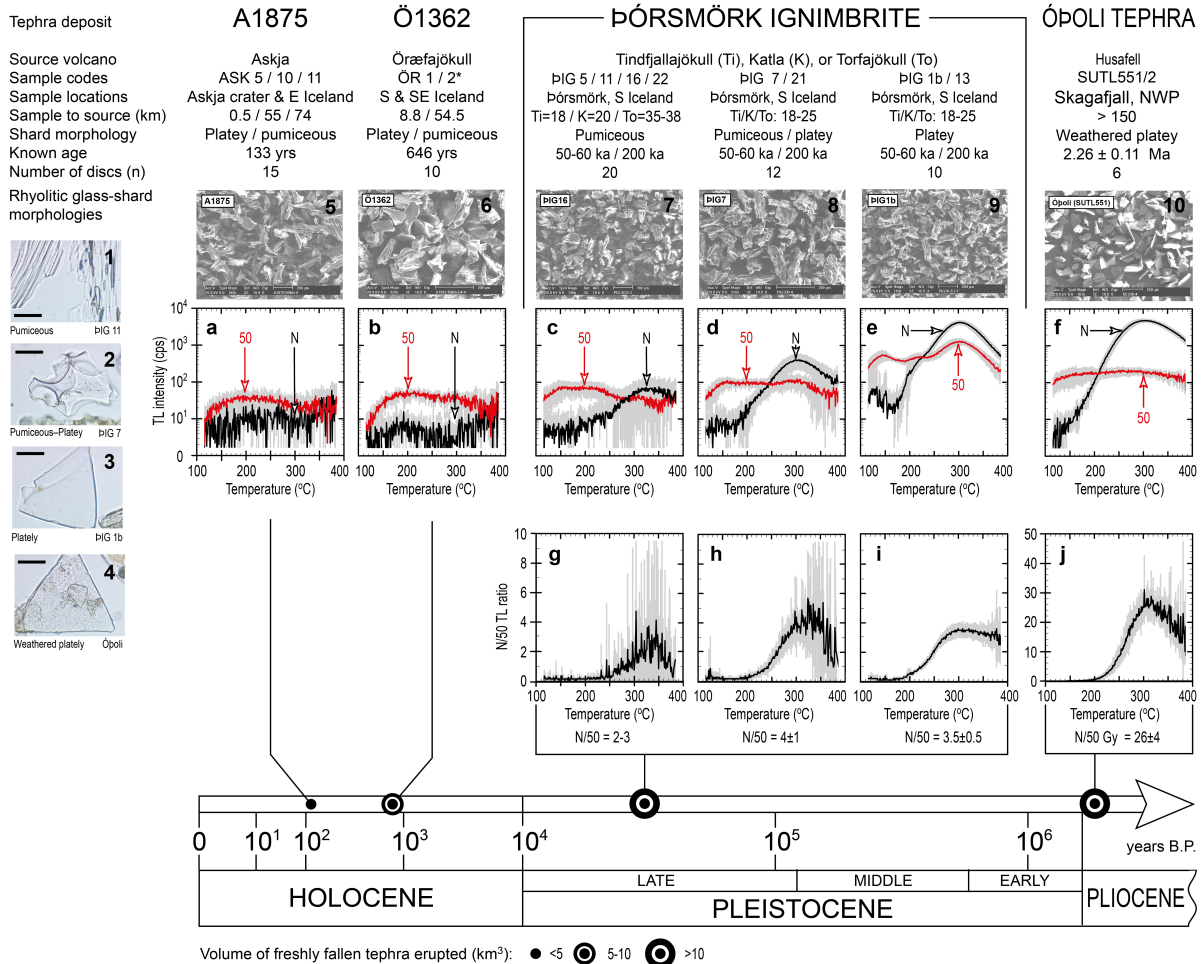
498 Using the purified 90-150 micron volcanic glass shard fraction of the four deposits, we
499 thermally read out the natural signal and examined their response to a 50 Gy radiation dose.
500 We also undertook TL bleaching, TL inducement and pre-heating tests (Figs. 6, S5;
501 Supplementary Notes 2, 3). Results showed an age-related signal was retained by volcanic
502 glass (Fig. 6), and that a fairly consistent volcanic glass-phase response to 50 Gy laboratory
503 radiation dose existed across all samples. This was characterised by a broad peak intensity
504 region of up to 10³–10⁴ counts per second (cps) between 200–400 °C (Fig. 6a-d, f). The natural
505 TL signal retained by the A1875 and Ö1362 samples was too small for further quantitative
506 analysis using the existing set up (Fig. 6). Bleaching and inducement tests showed the TL signal
507 could not be fully removed by optical exposure and that a TL signal of similar magnitude to
508 the natural Ópoli tephra signal could not induced by optical exposure. Manual pre-heats of
509 220 °C for two minutes, 155 °C for five hours or 135 °C for 16 hours all successfully removed
510 the laboratory-induced low temperature (c. 110 °C) TL peak observed in the natural and 50
511 Gy dose response experiment (Figs. 6, S5; see Supplementary Note 2 for experimental
512 details).

513

514 ***SAR-TL experiments & palaeodose reconstruction***

515 The Þórsmörk Ignimbrite ÞIG 7 purified glass sample was significantly more sensitive (defined
516 as TL intensity per unit applied dose) than the Ópoli Tephra sample and had a straightforward
517 linear dose response in the 200–400 °C temperature region (Figs. 7a, 8a). Notably, SAR-TL
518 regression curves used for final analysis of the ÞIG7 and the Ópoli Tephra samples had mean

519 r^2 values consistently >0.98 with $p < 0.0001$ in the 240–360 °C peak intensity region (Tables 1,
520 2).
521



522

523 **Figure 6. Preliminary natural versus 50 Gy (N/50 Gy) dose response tests for purified**

524 **volcanic glass samples. (a)–(f) black lines represent the mean natural TL intensity (N) in**

525 **counts per second (cps), at 1 °C intervals. Dark (red) lines represent the mean TL intensity**

526 **produced by applying a 50 Gy laboratory dose. Light grey lines are ± 1σ errors from n discs**

527 **shown at 1 °C intervals. Pre-heats were deliberately not applied prior to the N or 50 Gy TL**

528 **read outs to allow examination of the natural and dose response glow curve shape. This**

529 **creates a low temperature peak visible in some 50 Gy response profiles (e.g., ÞIG 1b and ÞIG**

530 **13). As no pre-heats or regression analysis were undertaken, the information contained in**

531 **this figure is not linked to age estimates obtained from the SAR-TL experiment. (g)–(j) Natural**

532 **and 50 Gy ratio plateau plots, showing the mean ratio and single standard deviation of the**

533 **N/50 Gy TL response; * = ÖR 3 was visibly contaminated by minerals unrelated to the eruption**

534 event and is not included for clarity. Microphotographs 1–4, taken at x400 magnification,
535 illustrate the difference between pumice and platey glass shard morphologies; black scale bar
536 is 25 μm ; purified samples were mounted in Canada Balsam. Scanning Electron Microscope
537 (SEM) microphotographs 5–10 show selected Ö1362, A1875, PIG7 and ÓT purified glass
538 shards on discs used in the preliminary N/50 Gy experiment. Discs were carbon coated for
539 SEM-EDS geochemical mapping causing low image resolution.

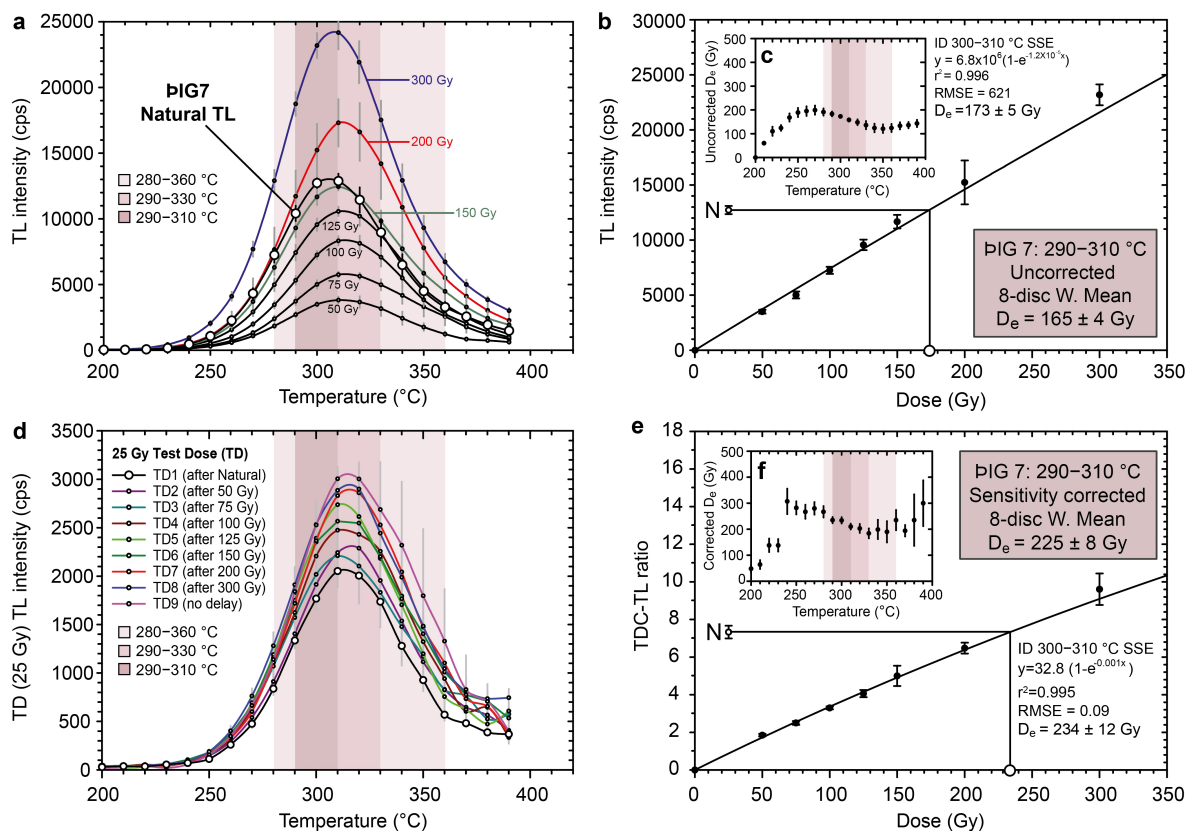
540

541 For PIG7, the uncorrected natural TL lies within an approximately linear growth phase of the
542 regeneration curve, enabling reliable D_e values to be obtained by interpolation (Fig. 7b).
543 Neither the type of regression curve fitted or the temperature integral chosen (280–360 °C ,
544 290–330 °C or 290–310 °C peak intensity regions of the glow curve) made a significant impact
545 on the reconstructed D_e value (Figure 7, Table 1). The PIG7 290–310 °C peak intensity region
546 had the most stable D_e plateau region with the lowest measurement errors (Fig. 7c) and was
547 chosen for D_e analysis. Uncorrected weighted linear (LIN) regression applied to 290–310 °C
548 data produced a D_e value of 169 ± 4 Gy, while weighted saturating exponential (SE) regression
549 produced a D_e of 165 ± 4 Gy (Fig. 7b; Table 1).

550

551 There was an approximately linear increase in TL intensity for PIG7 25 Gy test-doses TD1–TD9
552 (Fig. 6a–b). The PIG7 test-dose sensitivity-corrected 290–330 °C peak intensity weighted
553 mean D_e values were 221 ± 6 Gy (LIN) and 217 ± 5 Gy (SE) (Fig. 7e). Peak region (290–310 °C)
554 D_e values were similar (227 ± 8 Gy (LIN); 225 ± 8 Gy (SE)). Athermal fading did not appear to
555 be a significant for PIG7, with 96% of the signal retained in the 290–330 °C and 99% in the
556 290–310 °C stable peak temperature regions after 60-day storage (Tables 1, S3). Test-dose
557 (sensitivity) and 60-day storage loss-corrected SAR-TL D_e values across the 280–360 °C region

558 range from 226 ± 7 Gy to 234 ± 11 Gy (Table 1). The most accurate assessment of the PIG7
 559 palaeodose is considered to be the weighted mean sensitivity and 60-day storage-corrected
 560 SAR-TL D_e value of 230 ± 11 Gy, obtained by weighted linear regression from the 290–310 °C
 561 peak intensity temperature region (Table 1).



562
 563 **Figure 7. SAR-TL palaeodose (D_e) data for PIG 7 of the Þórsmörk Ignimbrite: (a)** Natural and
 564 applied dose mean TL intensity glow curves. Weighted mean TL intensity standard
 565 measurement errors were $10.48 \pm 1.32\%$ in the 280–360 °C peak intensity region, $5.93 \pm$
 566 0.66% for 290–330 °C and $5.95 \pm 0.95\%$ for 290–310 °C; **(b)** Example of a saturating
 567 exponential (SE) weighted regression curve fitting of the form $y=a[1-e^{(-bx)}]$ in the peak TL
 568 intensity 300-310 °C region. Similar SSE weighted regression was undertaken on 10-degree
 569 interval data between 200–400 °C to generate the D_e plateau plot shown in (c) (Tables 1, S2);
 570 **(c)** 200-400 °C D_e and temperature plateau plot; **(d)** 25 Gy test-dose (TD) mean TL intensity

571 glow curves; **(e)** Saturating exponential (SE) weighted regression of 300–310°C temperature
 572 test-dose (sensitivity)-corrected data (see also Fig. S6); **(f)** 200–400 °C D_e temperature test-
 573 dose (sensitivity) corrected D_e plateau plot. The weighted mean 290–310 °C sensitivity
 574 corrected $D_e = 225 \pm 8$ Gy. Results are based on 10 °C integration of original 1 °C data (Tables
 575 1, S2).

Þórsmörk Ignimbrite Palaeodose Statistics & Age estimates				Weighted mean age (no fading correction) $(D_{e, \text{glass-bulk}})_{\text{in-situ-sat}} = 5.82 \pm 1.48$ (ka)	60-day storage loss correction (Fraction of signal retained)	60-day storage loss corrected weighted mean palaeodose $D_e \pm SE$ (Gy)	60-day storage loss corrected weighted mean age $(D_{e, \text{glass-bulk}})_{\text{in-situ-sat}} = 5.82 \pm 1.48$ mGy a ⁻¹ (ka)	60-day storage loss corrected weighted mean age $(D_{e, \text{glass-bulk}})_{\text{in-situ-sat}} = 6.25 \pm 1.51$ mGy a ⁻¹ (ka)	
ÞIG7 SAR-TL		Weighted mean palaeodose $D_e \pm SE$ (Gy)	8-Disc Mean Regression Error Analysis (all $p < 0.0001$)						
	Mean $r^2 \pm 1\sigma$		Mean RMSE $\pm 1\sigma$						
Uncorrected	Linear regression								
	(a) 280-360 °C	157 ± 3	0.973 ± 0.025	639 ± 253	27 ± 7	0.94 ± 0.04	167 ± 8	29 ± 7	27 ± 7
	(b) 290-330 °C	166 ± 4	0.991 ± 0.009	527 ± 244	29 ± 7	0.96 ± 0.02	173 ± 5	30 ± 8	28 ± 7
	(c) 290-310 °C	169 ± 4	0.997 ± 0.003	352 ± 112	29 ± 7	0.99 ± 0.03	171 ± 7	29 ± 8	27 ± 7
	Saturating exponential regression								
	(d) 280-360 °C	151 ± 3	0.987 ± 0.009	511 ± 93	26 ± 7	0.94 ± 0.04	160 ± 8	28 ± 7	26 ± 6
(e) 290-330 °C	158 ± 3	0.995 ± 0.003	543 ± 62	27 ± 7	0.96 ± 0.02	165 ± 5	28 ± 7	26 ± 6	
(f) 290-310 °C	165 ± 4	0.997 ± 0.003	528 ± 65	28 ± 7	0.99 ± 0.03	167 ± 7	29 ± 7	27 ± 7	
Test dose- (Sensitivity)- corrected	Linear regression								
	(a) 280-360 °C	220 ± 5	0.984 ± 0.018	### ± 0.05	38 ± 10	0.94 ± 0.04	234 ± 11	40 ± 10	37 ± 9
	(b) 290-330 °C	221 ± 6	0.996 ± 0.004	### ± 0.03	38 ± 10	0.96 ± 0.02	231 ± 8	40 ± 10	37 ± 9
	(c) 290-310 °C	227 ± 8	0.999 ± 0.001	### ± 0.03	39 ± 10	0.99 ± 0.03	230 ± 11	39 ± 10	37 ± 9
	Saturating exponential regression								
	(d) 280-360 °C	215 ± 5	0.993 ± 0.009	### ± 0.06	37 ± 9	0.94 ± 0.04	229 ± 11	39 ± 10	37 ± 9
(e) 290-330 °C	217 ± 5	0.999 ± 0.001	### ± 0.04	37 ± 10	0.96 ± 0.02	226 ± 7	39 ± 10	36 ± 9	
(f) 290-310 °C	225 ± 8	0.999 ± 0.001	### ± 0.05	39 ± 10	0.99 ± 0.03	228 ± 10	39 ± 10	36 ± 9	

576

577 **Table 1. Summary palaeodose statistics and age estimates for the ÞIG7 sample.** The

578 weighted mean test-dose (sensitivity) and 60-day storage-loss corrected palaeodose and age

579 estimates shown in dark grey and in bold are considered to be reliable. Best fit regression

580 analysis was determined from highest adjusted r^2 values. Ten-degree integrated ranges for

581 the 280–360 °C, 290–330 °C and 290–310 °C TL peak intensity regions are shown. The 290–

582 310 °C and 290–330 °C ranges (dark grey shading) have the lowest TL intensity measurement

583 errors, the highest 8-disc mean r^2 , lowest RMSE values and lowest p -values. This produced

584 sensitivity and 60-day storage loss corrected palaeodoses of c. 230 ± 10 Gy and ages of 40 ±

585 10 ka. Data have been rounded to the nearest 10 Gy and 5 ka to reflect calculation errors,

586

587 In the 50 Gy dose response screening experiment, the natural TL signal from the Óþoli tephra

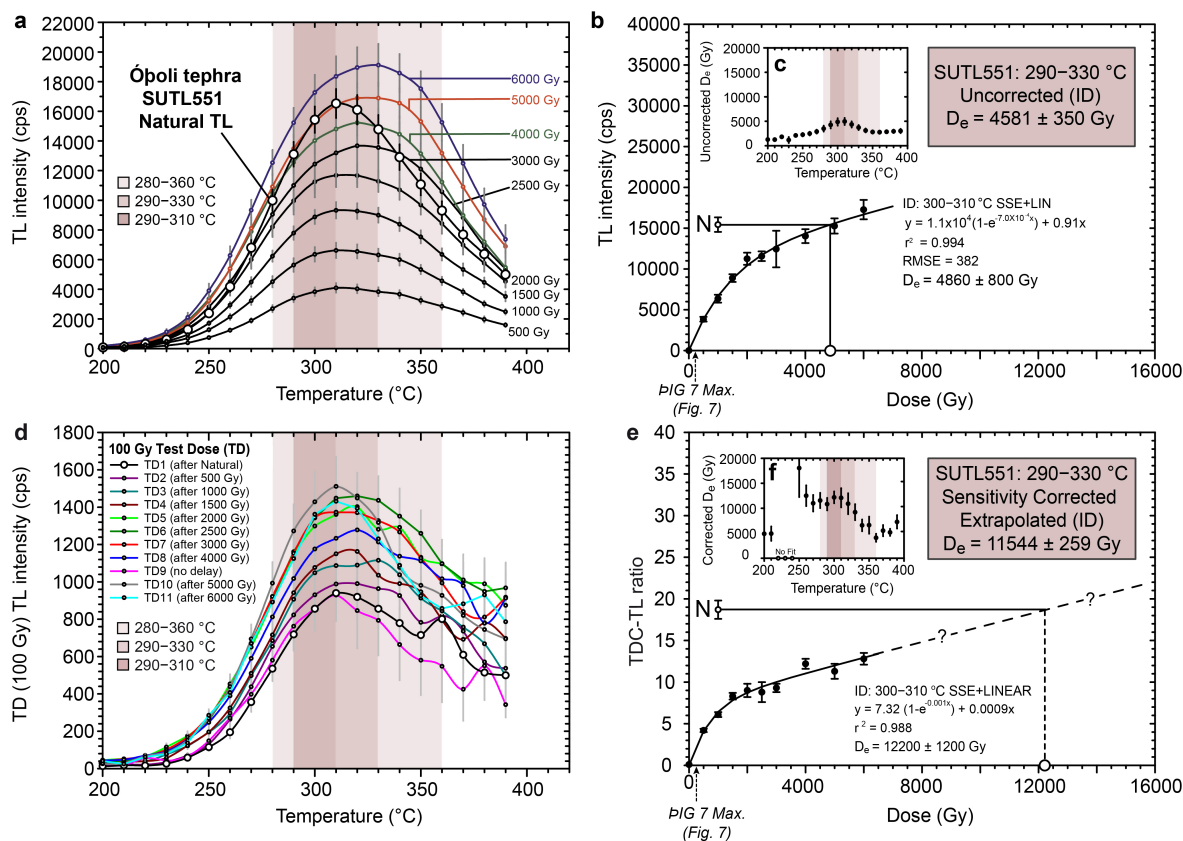
588 formed ‘broad’ unimodal peak of 10^3 – 10^4 cps °C⁻¹ between 280–360 °C (Fig. 6), indicating a

589 TL signal that is predominantly stored in the more stable, longer-term energy traps evicted at
590 high temperature. In the SAR-TL experiment, the uncorrected natural TL peak intensity region
591 of the glow curves from the Ópoli tephra (ÓT) covered a broader temperature range, 290–
592 330 °C, than PIG 7 (Fig. 8a). The broader shape of the regeneration dose response curve alone
593 implied that the ÓT was significantly older than the PIG7 sample (Fig. 8b). Regression results
594 show that the ÓT natural signal was located in an approximately linear growth phase *after* an
595 initial non-linear growth phase, best modelled by a saturating exponential plus linear
596 regression fit (Fig. 8b; Table S4). We chose this type of regression because it had a consistently
597 higher r^2 and lower RMSE values than single saturating exponential or polynomial (quadratic)
598 regression models (290–330 °C region mean $\pm 1\sigma$ $r^2 = 0.995 \pm 0.001$; $p < 0.0001$; Figs. 8b, S6;
599 Tables 2, S4). The 290–330 °C peak intensity region had the most stable D_e plateau, and
600 produced a weighted mean D_e value of 4581 ± 350 Gy (Fig. Table 2).

601

602 Assessing sensitivity change for the ÓT was more complex than for PIG7, with TL intensity
603 reversals between some adjacent 100 Gy test-dose runs (Fig. S6c–d). These non-linear effects
604 could be due to the (age-related) highly weathered and comparatively hydrated state of the
605 ÓT glass shards, the high laboratory dose rate, the higher magnitude of applied doses (>1
606 kGy), and/or cumulative radiation induced sensitivity changes (such as radiation ‘colouring’).
607 If the ÓT test-dose corrected response curve continued to grow in the same approximately
608 linear manner beyond 6 kGy, an applied dose in excess of 10 kGy would be required to
609 produce an interpolated sensitivity-corrected palaeodose estimate (Fig. 8e; Table 2). It was
610 not possible to apply such a high dose in the time available. Moreover, athermal fading
611 appeared to be a significant factor for the ÓT sample examined, with 73% the signal retained

612 in the 290–330 °C and 79% retained in the 290–310 °C stable peak temperature regions after
 613 60-day storage (Tables 2, S3).



614
 615 **Figure 8. SAR-TL D_e data for the Ópoli tephra airfall ash sample SUTL551: (a) Natural and**
 616 **applied dose mean TL intensity glow curves. Weighted mean uncorrected TL intensity**
 617 **measurement errors were 6.40 ± 0.11 % for the 280–360 °C peak intensity region, $6.37 \pm$**
 618 **0.06 % for 290–330 °C and 6.40 ± 0.13 % for 290–310 °C; (b) Example of a saturating**
 619 **exponential (SE) plus linear (LIN) weighted regression curve fitting $y = a[1 - e^{-bx}] + cx$ in the peak**
 620 **TL intensity 300–310 °C region. Similar SSE+LIN weighted regression was undertaken on 10**
 621 **degree interval data between 200–400 °C to generate the D_e plateau plot shown in (c) (Tables**
 622 **2, S4); (c) 200–400 °C D_e vs temperature plateau plot; (d) 100 Gy test-dose (TD) mean TL**
 623 **intensity glow curves; (e) SE+LIN weighted regression of 300–310 °C temperature peak region,**
 624 **highlighting how the reconstructed natural test-dose (sensitivity) corrected is greater than**

625 the highest applied dose of 6000 Gy (see also Fig. S6); **(f)** 200–400 °C (D_e) test-dose (sensitivity)
 626 corrected palaeodose (D_e) plateau plot. Results shown are based on 10 °C integrals with
 627 standard measurement error from measured 1 °C data (see also Tables 1, S3, S4).

Ópoli Tephra Palaeodose Statistics & Age estimates					Weighted mean age (no fading correction) $(D_T^{\text{glass-bulk}})_{\text{in-situ-sat}} 2.83 \pm$ (ka)	60-day storage loss correction (Fraction of signal retained)	60-day storage loss corrected weighted mean palaeodose $D_e \pm SE$ (Gy)	60-day storage loss corrected weighted mean age estimate $(D_T^{\text{glass-bulk}})_{\text{in-situ-sat}} 3.97 \pm 0.47$ (ka)	60-day storage loss corrected weighted mean age estimate $(D_T^{\text{glass-bulk}})_{\text{in-situ-sat}} 2.83 \pm$ (ka)
Ópoli Tephra (SUTL 551) SAR-TL		Weighted mean palaeodose	8-Disc Mean (8DM) Regression Error Analysis (all $p < 0.0001$)						
		$D_e \pm SE$ (Gy)	Mean $r^2 \pm 1\sigma$	Mean RMSE $\pm 1\sigma$					
Uncorrected	(a) 280-360 °C	3335 ± 155	0.995 ± 0.0015	331 ± 26	1178 ± 100	0.74 ± 0.03	4505 ± 278	1135 ± 90	1592 ± 149
	(b) 290-330 °C	4581 ± 350	0.995 ± 0.0012	342 ± 29	1619 ± 168	0.73 ± 0.02	6294 ± 511	1585 ± 151	2224 ± 239
	(c) 290-310 °C	4549 ± 524	0.995 ± 0.0002	355 ± 38	1607 ± 217	0.79 ± 0.01	5764 ± 668	1452 ± 184	2037 ± 277
Test-dose (Sensitivity) corrected	(a) 280-360 °C	8173 ± 153	0.986 ± 0.003	0.68 ± 0.13	2888 ± 211	0.74 ± 0.03	11040 ± 493	-	-
	(b) 290-330 °C	11544 ± 259	0.988 ± 0.003	0.58 ± 0.09	4079 ± 302	0.73 ± 0.02	15861 ± 562	-	-
	(c) 290-310 °C	11539 ± 302	0.986 ± 0.003	0.63 ± 0.09	4077 ± 307	0.79 ± 0.01	14622 ± 426	-	-

628

629 **Table 2. Summary palaeodose statistics and age estimates for the Ópoli tephra, sample.**

630 Ten-degree integrated intensity ranges for the three peak temperature plateau regions 280–
 631 360 °C, 290–330 °C and 290–310 °C are shown. The weighted mean sensitivity and 60-day
 632 storage loss-corrected palaeodose and age estimates highlighted in light grey overlap the
 633 fission-track age of 2.26 ± 0.11 Ma [75].

634

635 ***Dose rates and age estimates***

636 Environmental dose rates for PIG7, PIG1b and Ópoli tephra samples shown in Tables 3, 4 and
 637 S5 were produced using well-established equations and dose rate conversion factors. For
 638 PIG7, the spectrometry-based dose rate of 5.82 ± 1.48 mGy a^{-1} and geochemistry-based dose
 639 rate of 6.25 ± 1.51 mGy a^{-1} in combination with the sensitivity and 60-day storage loss-
 640 corrected palaeodose values of c. 230 ± 10 Gy produced age estimate of 40 ± 10 ka. High
 641 errors of c. 25% are mainly due to large uncertainties associated with estimating palaeowater
 642 content fluctuations. Due to erratic changes in sensitivity and unresolved, but significant,
 643 athermal signal losses, we cannot currently reconstruct a reliable SAR-TL age estimate for the
 644 Ópoli tephra sample. Interestingly, though, the minimum uncorrected age shown in Table 2

645 is 1178 ± 100 ka or 1.18 ± 0.1 Ma, and the 60-day storage loss-corrected SAR-TL D_e value of
 646 6294 ± 511 Gy and a geochemical dose-rate of 2.83 ± 0.41 mGy a^{-1} produces an age estimate
 647 of $2,224 \pm 239$ ka (2.22 ± 0.24 Ma) (Table 2), which is similar to the Ópöli tephra glass-shard
 648 fission-track age of 2.26 ± 0.11 Ma [75].

Geochemistry		Latitude	Longitude	Sampling	D_{cosmic}^1 dose rate (mGy a^{-1})	Elemental concentrations				
Tephra	Matrix	(°N)	(°W)	Depth (m)		n	K or K ₂ O* (wt %)	U (ppm)	Th (ppm)	Rb (ppm)
Pörsmörk Ignimbrite										
PIG 7	Bulk	63°40.37	19°34.37	1 ± 0.5	0.16 ± 0.06	-	3.03 ± 0.15	3.80 ± 0.19	13 ± 0.7	107 ± 5
	Glass					20	4.07 ± 0.19*	4.37 ± 0.22	14.3 ± 0.7	-
PIG 1b	Bulk	63°40.35	19°36.22	20 ± 5	0.04 ± 0.01	-	3.28 ± 0.16	3.13 ± 0.16	10 ± 0.5	73 ± 4
	Glass					24	4.11 ± 0.61*	3.39 ± 0.17	11.6 ± 0.6	-
Ópöli Tephra										
SUTL551/2	Bulk	65°59.78	23°45.40	5 ± 1	0.11 ± 0.04	-	2.16 ± 0.11	2.26 ± 0.03	8.5 ± 0.4	55 ± 3
	Glass					137	2.75 ± 0.14*	2.60 ± 0.10	10.8 ± 0.5	-

649

650 **Table 3. Location and geochemical data used to calculate dose rates for the Pörsmörk**
 651 **Ignimbrite and Ópöli tephra samples.** ¹The cosmic dose rate calculation assumes no change
 652 in sediment depth throughout burial and was calculated from $0.21e^{[-0.07(dr)+0.0005(dr)^2]}$ mGy
 653 a^{-1} [following 130] where d is current depth of burial and r is the density of the attenuating
 654 medium where $r = 0.998$ g cm^{-3} for water and 2.6 g cm^{-3} were used for sediment; n = number
 655 of shards analysed (Supplementary Note 1 and Table S1 for details).

Dose rate data		Glass shard dose rates					Bulk matrix dose rates					Weighted mean
Tephra	Measurement	D_{α_T}	D_{β_T}	D_{γ_T}	D_{cos}	$(D_T^{\text{glass}})_{(in-situ\ to\ sat)}$	D_{α_T}	D_{β_T}	D_{γ_T}	D_{cos}	$(D_T^{\text{bulk}})_{(in-situ\ to\ sat)}$	$(D_T^{\text{glass-bulk}})_{(in-situ\ to\ sat)}$
Lab ID	technique	(mGy a^{-1})				(mGy a^{-1})	(mGy a^{-1})				(mGy a^{-1})	
Pörsmörk Ignimbrite												
PIG 7	α -dose excluded	-	-	-	-	-	-	2.81	1.07	0.16	2.85 ± 0.60	2.85 ± 0.60
	Spectrometry*	1.84	2.12	1.09	0.16	5.22 ± 2.11	3.04	2.12	1.07	0.16	6.39 ± 2.07	5.82 ± 1.48
	Geochemical	1.84	2.09	1.09	0.16	5.18 ± 2.38	3.04	3.32	1.09	0.16	6.97 ± 1.96	6.25 ± 1.51
PIG 1b	α -dose excluded	-	-	-	-	-	-	2.55	1.09	0.05	2.96 ± 0.57	2.96 ± 0.57
	Spectrometry*	1.72	1.91	1.11	0.04	4.78 ± 2.12	2.43	1.91	1.09	0.05	5.48 ± 2.03	5.14 ± 1.47
	Geochemical	1.71	2.30	1.11	0.05	5.17 ± 2.64	2.43	3.12	1.11	0.05	6.71 ± 2.14	6.10 ± 1.66
Ópöli Tephra												
	α -dose excluded	-	-	-	-	-	-	1.59	0.56	0.11	1.83 ± 0.17	1.83 ± 0.17
	Spectrometry*	1.30	1.11	0.30	-	2.70 ± 0.62	1.51	1.11	0.30	-	2.92 ± 0.54	2.83 ± 0.41
	Geochemical	1.30	1.65	0.85	0.11	3.90 ± 0.66	1.51	1.58	0.85	0.11	4.04 ± 0.67	3.97 ± 0.47

656

657 **Table 4. Summary dose rate data for the Pörsmörk Ignimbrite and Ópöli tephra samples.**
 658 Summary dose rate values were calculated with α -dose rate excluded, using spectrometry
 659 data (α -dose included) and using geochemical data (α -dose included) for three scenarios:

660 glass shard, bulk matrix, and weighted mean (glass shard–bulk) matrix. Values in bold are
661 considered most likely. For geochemical calculations, the glass shard matrix dose rate was
662 calculated using well-established equations and conversion factors [107–109, 130–133]. Since
663 the biggest source of uncertainty is variations in palaeowater content, using more recent
664 conversion factors does not significantly alter these calculated dose rates or errors. Total
665 alpha, beta and gamma dose rates ($D\alpha_T$, $D\beta_T$, $D\gamma_T$) incorporate attenuation factors based on
666 *in situ*–saturation water content values [105, 132], which we consider to be most
667 representative of the average water content through burial history at both the ÞIG 7 and Óþoli
668 tephra sites (see Methods, Table S5). D_{cos} is the cosmic dose rate shown in Table 3. Errors for
669 dose rate components are not shown for clarity but are typically $\pm 10\%$.

670

671 **Discussion**

672 We discuss the accuracy of the new ÞIG7 TL age estimate, examine implications of the age
673 obtained, and make suggestions for future TL analysis of glass-rich tephra deposits based on
674 the results from the ÞIG7 and Óþoli tephra experiments.

675

676 **Experimental Implications**

677 Our experiments on the Þórsmörk Ignimbrite (ÞIG7) produced age estimates that were similar
678 orders of magnitude to published ages, highlighting that a glass-formation age-related TL
679 signal is retained by the rhyolitic volcanic glass component of Icelandic tephra. In palaeodose
680 reconstruction, even the smallest laboratory doses are applied at rates which are several
681 orders of magnitude greater than those experienced in the natural environment. This creates
682 two problems. First, high laboratory doses tend to fill or saturate shallow, thermally unstable
683 traps, a process which does not occur during slower natural irradiation processes and may

684 result in differences in deep trap sensitivity [99, 110, 111]. Second, although laboratory dose
685 rates less than c. 10 Gy min^{-1} are not thought to be problematic [100], studies have shown
686 that laboratory irradiation at 10^8 – 10^{11} (c. 0.1 – 100 Gy min^{-1}) times greater than that
687 experienced in the natural environment can lead to defect creation, migration and,
688 ultimately, defect complex creation, which does not occur naturally [121]. Glass should be
689 one of the materials least affected, because localised charge transport is not favourable for
690 shallow-deep trap competition. The erratic sensitivity changes observed for the Ópoli tephra
691 in the SAR-TL experiment suggest the comparatively higher laboratory dose rates (an order
692 of magnitude greater than for the PIG7 sample) were detrimental in this respect. The obvious
693 solution is to reduce the applied dose rate, but this would be extremely time consuming for
694 multiple discs with several applied doses runs $>1000 \text{ Gy}$.

695

696 Further investigation into the influence of sample age and applied dose on athermal signal
697 loss is recommended. This effect was minimal for the PIG sample but appears to be a
698 significant issue for the much older Ópoli tephra, which received applied doses in the c. 1-6
699 kGy range. From our investigations, the athermal signal loss characteristics of ‘younger’
700 volcanic glass deposits appears to be similar to those of commercial glasses, which do not
701 exhibit significant athermal losses at ‘low’ applied doses i.e., $<100 \text{ kGy}$ [66]. Compositional
702 differences, additional lattice defects and/or weathering could explain the lower dose
703 threshold observed in our experiments.

704

705 Athermal fading of stored TL in phenocrysts of volcanic origin is thought to be responsible for
706 significant D_e underestimates in OSL dating of quartz phenocrysts present in some tephra
707 deposits from Japan [112, 114, 115] and infra-red stimulated luminescence (IRSL) dating of

708 volcanic feldspar and other phenocrysts in the Old Crow Tephra, Alaska [113]. 'Young' volcanic
709 glass shards appear less susceptible to long-term athermal signal loss at low irradiation doses
710 [65, 66, 110-115], perhaps because fewer opportunities for long-range charge transport exist
711 in volcanic glass compared to mineral-based luminescence systems. The relatively small TL
712 signals per unit dose and low short-range order of glasses may also result from increased
713 opportunities for competing non-radiative relaxation. At low doses, recombination is most
714 likely to take place in hole centres populated from non-correlated ionising events, leading to
715 the type of reproducible dose response curves observed in the PIG7 sample. At higher doses
716 (*e.g.*, >1 kGy) [66], the increased proximity between donors and acceptors pair may eventually
717 favour tunnelling recombination and limit stability, as seen by the greater athermal losses in
718 the Ópoli tephra.

719

720 By calculating the ionisation density as a function of dose and partitioning the dose (energy
721 per unit mass) amongst the atoms in feldspar, Sanderson [116] showed that the mean spacing
722 of randomly positioned charge-carriers in a lattice irradiated at low doses was greater than
723 1000 lattice units. The random spatial model for fading in calcite [117], which has been
724 subsequently applied to feldspars [116, 118], other minerals [119], and volcanic products
725 [120] is perhaps less relevant for volcanic glass since it cannot support high rates of tunnelling
726 at low dose without some form of charge-defect clustering, leading to deviations from the
727 logarithmic ($1/t$) decay behaviour predicted by the Visocekas [117] model. Ward [67] showed
728 that fading from glass cover slips across a range of doses up to 160 kGy exhibits logarithmic
729 ($1/t$) decay behaviour only at the highest doses used. At very high doses, the proximity of
730 neighbouring ion pairs becomes sufficiently close to enable anomalous signal losses from the
731 glass matrix by quantum mechanical tunnelling [cf. 116], as observed by high dose

732 experiments from glass slices [66, 67, 111]. In fact, all materials should exhibit (quantum
733 mechanical) tunnelling as the mean concentration of electron-ion pairs reaches the percent
734 level. If 1 kGy corresponds to 10 ppm initial ionisation, the mean concentration of electron-
735 ion pairs reaches the percent level at doses in the 10's-100's kGy region. At low doses, thermal
736 fading occurs from the continuum of traps where charge is located, and is presumably lost to
737 non-luminescence processes, but this is not necessarily a significant barrier to successful
738 dating providing the stability of the signal can be demonstrated by, for example, the existence
739 of stable thermal plateau plots.

740

741 In early work examining a range of glass-rich tephras Berger [73,74], expressed concern that
742 feldspar phenocrysts had potential to dominate fading behaviour for impure samples. He
743 noted the apparent stability of the glass rich tephra from the Mazama, tephra and suggested
744 that the glass phase experienced long-term athermal fading. Following the demonstration
745 that tephra showed weak OSL and IRSL response [75], Auclair [113] studied the potential of
746 IRSL dating from Crow Lake tephra from Alaska, in conjunction with stratigraphically
747 associated loess. The tephra samples, which had not been subject to flotation, had IRSL signals
748 which were an order of magnitude lower than the glass rich fractions, but, unlike samples used
749 in this study, retained plagioclase as well as volcanic glass, pyroxene and iron oxides. Three
750 approaches to fading analysis over a timescale ranging from 16 hours to 2000 hours were
751 examined, with differing results. When aliquots were irradiated and staggered intervals and
752 read together at the end of the storage period (to minimise the effects of sensitivity change
753 in readout equipment), scattered results were obtained, with a mean value of 2% fading per
754 decade of time. The use of short IRSL measurements, which scarcely depleted individual
755 aliquots, allowed multiple measurement from individual samples, and produced more

756 coherent data. Fading rates of 4% and 6% per decade were obtained from loess and tephra
757 samples, which are within uncertainties of each other. These values are very similar to values
758 obtained from feldspars. Auclair [113] noted the possibility that they may relate to the
759 phenocrysts in the sample, rather than the glass phase, and also noted the possible ambiguity
760 between fading and sensitivity change in the experimental design.

761

762 While our experiments suggest that the purification of coarser material from both PIG7 and
763 the Ópoli tephra was more successful, at this stage, it is not clear if storage signal losses
764 observed from the Ópoli tephra were due to insufficient thermal stability in the temperature
765 range examined, the onset of proximity effects or possibly related to the increased level of
766 weathering experienced by this sample over time. Despite low luminescence sensitivities, the
767 signal obtained from synthetic glasses continued to grow in a similar approximately linear
768 fashion after near-saturation to the Ópoli tephra [67]. This implies that dating of volcanic glass
769 up to at least two million years old could be possible, but several technical refinements are
770 needed to obtain accurate and reliable ages. Further high-dose experiments on volcanic glass
771 of Quaternary age and different geochemical composition are recommended to determine if
772 signal loss is related to burial age, geochemical composition and/or the scale of laboratory
773 doses or dose rates.

774

775 The other key factor in assessing the reliability of age estimates is the accuracy of calculated
776 dose rates. The large age errors in this study relate to the large dose rate errors and are
777 primarily due to long-term variations in palaeowater content during burial. However, our
778 dose rate calculations also had to account for variations in the alpha dose contribution since
779 it was not possible to etch the thin platy glass shards without destroying them. The alpha

780 dose contributed as much as 50% of the total dose rate in this study and creates uncertainties
781 that are as significant as those associated with changes in palaeowater content (Table 4). The
782 observed similarity between bulk and internal glass-shard compositions in both samples
783 examined suggests that sharp micro-dosimetric discontinuities probably do not exist at shard
784 boundaries. Nevertheless, whilst we constrained alpha dose-related uncertainties as far as
785 currently feasible, alpha dose attenuation in irregularly shaped glass shards could be
786 significantly different to published dosimetric equations, which are based on spherical grains
787 [100, 108, 122, 123]. Numerical modelling, beyond the scope of this paper, is therefore
788 recommended to fully evaluate the dosimetric properties of glass shard shapes that are not
789 perfect spheres. An in-depth comparison with dose rates from tephra deposits where volcanic
790 glass constitutes less than c. 95% of the bulk tephra matrix might also be useful.

791

792 In summary, we conclude that sensitivity and long-term storage tests are critical components
793 that should be included in all future analyses. Further reducing uncertainties associated with
794 our age estimates would also require extensive *in-situ* dose rate measurements, including for
795 example, a better assessment of seasonal to multi-decadal fluctuations in water content at
796 each site. Automation, single-grain glass shard analysis (where sensitivity allows) and pulsed-
797 laser infra-red stimulated luminescence (IRSL) methods could be applied and compared to
798 ages obtained from feldspar-phenocryst phases in glass-rich deposits. This could result in
799 reliable TL ages from tephra across a broad age-spectrum, up to and beyond the radiocarbon
800 dating upper limit of c. 50 ka.

801

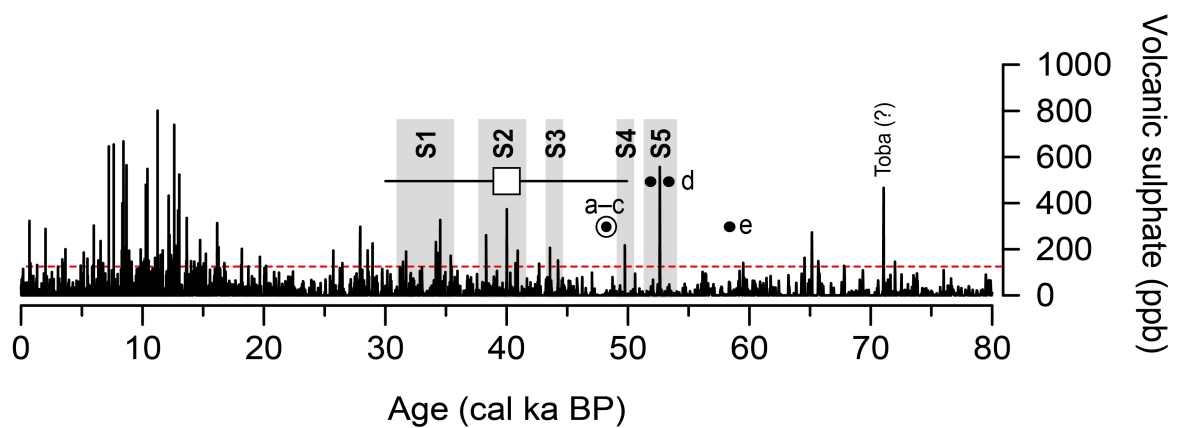
802 ***Palaeoenvironmental Implications***

803 The c. 40 ± 10 ka age estimate of the PIG7 sample is similar in magnitude to existing age
804 estimates obtained from the Þórsmörk region. It is also a closer approximation to ‘known’
805 ages for this deposit than, for example, the glass-phase TL age of 23.4 ± 2.4 ka obtained from
806 deposits associated with the c. 75 ka Toba eruption [124]. Post depositional thermal annealing
807 of the PIG7 sample could have reduced its measured age, but there are no currently active
808 thermal areas in the Þórsmörk valley. Our c. 40 ± 10 ka age estimate also eliminates the
809 possibility of a c. 200 ka eruption age for deposits at the PIG7 site. Following the SAR-TL
810 experiments, we examined glass shards in the PIG1b and PIG7 samples for the presence of
811 spontaneous fission-tracks. None were observed. The absence of natural fission-tracks in
812 volcanic glass with a c. 3–4.5 ppm uranium and c. 10–14.5 ppm thorium content provides an
813 additional age constraint of $< c.100$ ka, and rules out the possibility of a c. 200 ka eruption age
814 in more than one location within the Þórsmörk valley.

815

816 The 40 ± 10 ka age is potentially younger than the established age of NAAZ2 and raises the
817 intriguing possibility of multiple ignimbrite- or rhyolitic-ash forming eruptions in the area
818 between 60–30 ka. Lacasse et al. [2, 4] first suggested the PIG is the terrestrial geochemical
819 equivalent of North Atlantic Ash Zone 2 (NAAZ-2). NAAZ-2 was originally dated in marine cores
820 to around 64 ka [46]. Later, correlation ages of 48.5–58 ka were proposed by comparing the
821 astronomically calibrated oxygen isotope time scale from marine cores with the Greenland
822 GISPII ice core incremental timescale [9, 86]. The widespread distribution of the Vedde Ash
823 and NAAZ-II in marine cores of the North Atlantic has been linked with ice rafting [9, 46],
824 raising doubts over the precision of c. 64–48 ka correlation ages for NAAZ-II in marine cores.
825 The spread of ages within NAAZ-II could also indicate more than one eruption event. Zielinski
826 et al. [9] proposed that NAAZ-II was the result of two simultaneous eruptions from Katla and

827 Torfajökull based on two distinct tephra deposits with similar chemical composition to NAAZ-
 828 II and the PIG found in Greenland ice cores at 53.5 ka and 57.3 ka [86, 87] (Fig. 9). The c. 40
 829 ka age estimate for the PIG7 sample is approximately 23% younger these ice core ages, but
 830 coeval with an elevated volcanic sulphate peak in the GISP2 ice core record centred on 40 ka
 831 (Fig. 9). Moreover, the tephrochronology of 60-30 ka eruptions from Iceland has recently
 832 been geochemically mapped in unprecedented detail and supports the possibility of multiple
 833 large rhyolite-forming eruptions from volcanic complexes in and around Þórsmörk during this
 834 period.



835 □ PIG7 SAR-TL age S1–S5 Volcanic sulphate >126 ppb (99% percentile) in SAR-TL range
 ● Closest geochemical correlation match • Geochemical correlation match

836 **Figure 9 The GISP2 Volcanic Sulphate record of palaeovolcanism for the last 80,000 years**
 837 **compared to new SAR-TL age estimates for Þórsmörk Ignimbrite.** Notes: IC ka = ice core
 838 years before present; References: (a) [53]; (b), (c) [2, 4]; (d) [9]; (e) [46].

839
 840 To summarise, TL screening and dating of volcanic glass in tephra holds great potential,
 841 particularly for the rapid classification of geochemically similar volcanic systems with widely
 842 separated eruption events. Whether all the ignimbrite deposits in the Þórsmörk area are from
 843 the same eruption event remains uncertain and warrants further investigation. Luminescence

844 and radiometric dating of other deposits in the Þórsmörk area is recommended to determine
845 if more than one ignimbrite-forming eruption event occurred between 60-30 ka and further
846 improve the tephrochronological record of Iceland.

847

848 **Conclusions**

849 1) To improve the Late Pleistocene tephrochronology of Iceland, NW Europe, and the North
850 Atlantic and Arctic regions, we investigated the thermoluminescence (TL) dose response
851 characteristics of rhyolitic volcanic glass produced by four large Plinian eruptions from
852 Iceland: the c. 50 ka Þórsmörk Ignimbrite, Askja 1875 AD, Öræfi 1362 AD and the Late Pliocene
853 Óþoli Tephra,

854

855 2) Our screening experiments showed an unequivocal age-related increase in naturally
856 retained glass-phase TL. Single aliquot regeneration-TL analysis of volcanic-glass from the
857 Þórsmörk Ignimbrite produced an age estimate of c. 40 ± 10 ka, supporting evidence for a
858 major eruption in the Þórsmörk area of Southern Iceland 30–60 ka rather than c. 200 ka.

859

860 3) The application of combined glass-phase thermoluminescence and radiometric dating at
861 multiple sites in the Þórsmörk area could reveal if more than one ignimbrite-forming eruption
862 occurred between 30-60 ka. Results from the Óþoli tephra were a similar order of magnitude
863 to its established c. 2 Ma age, but further investigation of sensitivity change and signal loss
864 from 'older' volcanic glass deposits is required. The tephrochronological record of Iceland
865 could be improved using TL analysis of volcanic glass deposits.

866

867

868 **Acknowledgements**

869 SJR, AJD and DCWS undertook fieldwork funded by National Environmental Research Council
870 (NERC) Grant no. GT 04/97/85/ES and the University of Edinburgh Moray Endowment Fund
871 and Small Projects Grant; DCWS provided access to and support with luminescence analysis
872 and interpretation. AJD acknowledges support of the National Science Foundation of America
873 grant 1249313. SJR acknowledges additional support from BAS. The funders had no role in
874 study design, data collection and analysis, decision to publish, or preparation of the
875 manuscript. Thanks to Rob Austin-Smith, Tom Bradwell, Jeremy Everest and Bob McCulloch
876 for their assistance in the field, John Westgate for examining Þórsmörk Ignimbrite ÞIG 1b and
877 ÞIG7 samples for fission-tracks, Peter Hill, Paula McDade, Anthony Newton, and Shari Preece
878 for assistance with geochemical analysis. The authors have no competing interests. All
879 necessary permits were obtained for the described study, which complied with all relevant
880 regulations.

881

882 **Data availability**

883 Datasets are summarised in the Supplementary Material, are available from the
884 corresponding author (sjro@bas.ac.uk) and these links:

885 Supplementary material: <https://doi.org/10.6084/m9.figshare.13634666.v1>

886 Datasets: <https://doi.org/10.6084/m9.figshare.13633877.v1>,

887

888 **References**

- 889 1. Thórarinsson S. Ignimbrit í Þórsmörk. (Ignimbrite in Þórsmörk). Náttúrufræðingurinn.
890 1969;39:139-55.
- 891 2. Lacasse C, Sigurdsson H, Johannesson H, Paterne M, Carey S. Source of Ash-Zone-1 in
892 the North-Atlantic. Bulletin of Volcanology. 1995;57(1):18-32.
893 doi:10.1007/Bf00298704. PubMed PMID: WOS:A1995RB63400002.
- 894 3. Sigurdsson H, McIntosh WN, Dunbar N, Lacasse C, Carey SN. Thorsmörk ignimbrite in
895 Iceland: possible source of North Atlantic Ash Zone 2. EOS Trans American Geophysical
896 Union, Boston, 26-29 May 1998. 1998;EOS Trans. AGU, Spring Meet.
897 Suppl.(79(17)):S172.
- 898 4. Lacasse C, Sigurdsson H, Carey S, Paterne M, Guichard F. North Atlantic deep-sea
899 sedimentation of Late Quaternary tephra from the Iceland hotspot. Marine Geology.
900 1996;129(3-4):207-35. doi:10.1016/0025-3227(96)83346-9. PubMed PMID:
901 WOS:A1996TV77400003.
- 902 5. Blockley SPE, Bourne AJ, Brauer A, Davies SM, Hardiman M, Harding PR, et al.
903 Tephrochronology and the extended intimate (integration of ice-core, marine and
904 terrestrial records) event stratigraphy 8–128 ka b2k. Quaternary Science Reviews.
905 2014;106:88-100. doi: <http://dx.doi.org/10.1016/j.quascirev.2014.11.002>.
- 906 6. Thórarinsson S. Askja on fire. Reykjavík: Almenna Bókafélagid; 1963.
- 907 7. Dugmore AJ. Tephrochronological studies of Holocene glacier fluctuations in south
908 Iceland. In: Oerlemans J, editor. Glacier fluctuations and climatic change: Kluwer
909 Academic Publishers; 1989. p. 37-55.
- 910 8. Zielinski GA, Germani MS, Larsen G, Baillie MGL, Whitlow S, Twickler MS, et al. Evidence
911 of the Eldgja (Iceland) Eruption in the Gisp2 Greenland Ice Core - Relationship to
912 Eruption Processes and Climatic Conditions in the 10th-Century. Holocene.
913 1995;5(2):129-40. doi:10.1177/095968369500500201. PubMed PMID:
914 WOS:A1995RB22100001.

- 915 9. Zielinski GA, Mayewski PA, Meeker LD, Gronvold K, Germani MS, Whitlow S, et al.
916 Volcanic aerosol records and tephrochronology of the Summit, Greenland, ice cores.
917 *Journal of Geophysical Research-Oceans*. 1997;102(C12):26625-40.
918 doi:10.1029/96jc03547. PubMed PMID: WOS:A1997YJ67100027.
- 919 10. Dugmore AJ, Newton AJ, Edwards KJ, Larsen G, Blackford JJ, Cook GT. Long-distance
920 marker horizons from small-scale eruptions: British tephra deposits from the AD 1510
921 eruption of Hekla, Iceland. *Journal of Quaternary Science*. 1996;11(6):511-6. doi:
922 10.1002/(Sici)1099-1417(199611/12)11:6<511::Aid-Jqs284>3.0.Co;2-C. PubMed PMID:
923 WOS:A1996WE01200006.
- 924 11. Larsen G, Dugmore A, Newton A. Geochemistry of historical-age silicic tephtras in
925 Iceland. *Holocene*. 1999;9(4):463-71. doi:10.1191/095968399669624108. PubMed
926 PMID: WOS:000081526000007.
- 927 12. Wastegard S, Wohlfarth B, Subetto DA, Sapelko TV. Extending the known distribution
928 of the Younger Dryas Vedde Ash into northwestern Russia. *Journal of Quaternary
929 Science*. 2000;15(6):581-6. doi:10.1002/1099-1417(200009)15:6<581::Aid-
930 Jqs558>3.3.Co;2-V. PubMed PMID: WOS:000089379900003.
- 931 13. Wastegard S, Turney CSM, Lowe JJ, Roberts SJ. New discoveries of the Vedde Ash in
932 southern Sweden and Scotland. *Boreas*. 2000;29(1):72-8. PubMed PMID:
933 WOS:000086023300006.
- 934 14. Wastegard S, Rasmussen TL. New tephra horizons from Oxygen Isotope Stage 5 in the
935 North Atlantic: correlation potential for terrestrial, marine and ice-core archives. *Quat
936 Sci Rev*. 2001;20(15):1587-93. doi:10.1016/S0277-3791(01)00055-5. PubMed PMID:
937 WOS:000171249500002.
- 938 15. Wastegard S, Hall VA, Hannon GE, van den Bogaard C, Pilcher JR, Sigurgeirsson MA, et
939 al. Rhyolitic tephra horizons in northwestern Europe and Iceland from the AD 700s-
940 800s: a potential alternative for dating first human impact. *Holocene*. 2003;13(2):277-
941 83. doi: 10.1191/0959683603hl617rr. PubMed PMID: WOS:000181279000011.
- 942 16. Wastegard S, Bjorck S, Greve C, Rasmussen TL. A tephra-based correlation between the
943 Faroe Islands and the Norwegian Sea raises questions about chronological relationships
944 during the last interglacial. *Terra Nova*. 2005;17(1):7-12. doi: 10.1111/j.1365-
945 3121.2004.00578.x. PubMed PMID: WOS:000227350400002.
- 946 17. Wastegard S. Late Quaternary tephrochronology of Sweden: a review. *Quaternary
947 International*. 2005;130:49-62. doi: 10.1016/j.quaint.2004.04.030. PubMed PMID:
948 WOS:000226424200005.
- 949 18. Wastegard S, Rasmussen TL, Kuijpers A, Nielsen T, van Weering TCE. Composition and
950 origin of ash zones from Marine Isotope Stages 3 and 2 in the North Atlantic. *Quat Sci
951 Rev*. 2006;25(17-18):2409-19. doi: 10.1016/j.quascirev.2006.03.001. PubMed PMID:
952 WOS:000240819000024.
- 953 19. Rasmussen TL, Wastegard S, Kuijpers E, van Weering TCE, Heinemeier J, Thomsen E.
954 Stratigraphy and distribution of tephra layers in marine sediment cores from the Faeroe
955 Islands, North Atlantic. *Marine Geology*. 2003;199(3-4):263-77. doi: 10.1016/S0025-
956 3227(03)00219-6. PubMed PMID: WOS:000185176400004.
- 957 20. Wallrabe-Adams HJ, Lackschewitz KS. Chemical composition, distribution, and origin of
958 silicic volcanic ash layers in the Greenland-Iceland-Norwegian Sea: explosive volcanism
959 from 10 to 300 ka as recorded in deep-sea sediments. *Marine Geology*. 2003;193(3-
960 4):273-93. doi: Pii S0025-3227(02)00661-8 Doi 10.1016/S0025-3227(02)00661-8.
961 PubMed PMID: WOS:000181296600007.

- 962 21. Davies SM, Branch NP, Lowe J, Turney CSM. Towards a European tephrochronological
963 framework for termination 1 and the early holocene. *Philosophical Transactions of the*
964 *Royal Society of London Series a-Mathematical Physical and Engineering Sciences.*
965 2002;360(1793):767-802. doi: 10.1098/rsta.2001.0964. PubMed PMID:
966 ISI:000175121800010.
- 967 22. Davies SM, Wastegard S, Wohlfarth B. Extending the limits of the Borrobol Tephra to
968 Scandinavia and detection of new early Holocene tephras. *Quaternary Research.*
969 2003;59(3):345-52. doi: 10.1016/S0033-5894(03)00035-8. PubMed PMID:
970 WOS:000183386500007.
- 971 23. Davies SM, Wastegard S, Rasmussen TL, Svensson A, Johnsen SJ, Steffensen JP, et al.
972 Identification of the Fugloyarbanki tephra in the NGRIP ice core: a key tie-point for
973 marine and ice-core sequences during the last glacial period. *Journal of Quaternary*
974 *Science.* 2008;23(5):409-14. doi: 10.1002/jqs.1182. PubMed PMID:
975 WOS:000257958100002.
- 976 24. Davies SM, Abbott PM, Pearce NJG, Wastegard S, Blockley SPE. Integrating the
977 INTIMATE records using tephrochronology: rising to the challenge. *Quat Sci Rev.*
978 2012;36:11-27. doi: 10.1016/j.quascirev.2011.04.005. PubMed PMID:
979 WOS:000301825900003.
- 980 25. Davies SM, Abbott PM, Meara RH, Pearce NJG, Austin WEN, Chapman MR, et al. A North
981 Atlantic tephrostratigraphical framework for 130–60 ka b2k: new tephra discoveries,
982 marine-based correlations, and future challenges. *Quaternary Science Reviews.*
983 2014;106:101-21. doi: <http://dx.doi.org/10.1016/j.quascirev.2014.03.024>.
- 984 26. Pyne-O'Donnell SDF. Three new distal tephras in sediments spanning the Last Glacial-
985 Interglacial Transition in Scotland. *Journal of Quaternary Science.* 2007;22(6):559-70.
986 doi: 10.1002/jqs.1066. PubMed PMID: WOS:000249439600001.
- 987 27. Pyne-O'Donnell SDF, Blockley SPE, Turney CSM, Lowe JJ. Distal volcanic ash layers in the
988 Lateglacial Interstadial (GI-1): problems of stratigraphic discrimination. *Quat Sci Rev.*
989 2008;27(1-2):72-84. doi: 10.1016/j.quascirev.2007.02.019. PubMed PMID:
990 WOS:000254196600007.
- 991 28. Beget JE, Keskinen MJ. Trace-element geochemistry of individual glass shards of the Old
992 Crow tephra and the age of the Delta glaciation, central Alaska. *Quaternary Research.*
993 2003;60(1):63-9. doi: 10.1016/S0033-5894(03)00095-4. PubMed PMID:
994 WOS:000184258400008.
- 995 29. Dugmore AJ, Larsen G, Newton AJ. 7 Tephra Isochrones in Scotland. *Holocene.*
996 1995;5(3):257-66. doi:10.1177/095968369500500301. PubMed PMID:
997 WOS:A1995RW28900001.
- 998 30. Pearce NJG, Alloway BV, Westgate JA. Mid-Pleistocene silicic tephra beds in the
999 Auckland region, New Zealand: Their correlation and origins based on the trace element
1000 analyses of single glass shards. *Quaternary International.* 2008;178:16-43. doi:
1001 10.1016/j.quaint.2006.09.005. PubMed PMID: WOS:000255304900005.
- 1002 31. Pearce NJG, Denton JS, Perkins WT, Westgate JA, Alloway BV. Correlation and
1003 characterisation of individual glass shards from tephra deposits using trace element
1004 laser ablation ICP-MS analyses: current status and future potential. *Journal of*
1005 *Quaternary Science.* 2007;22(7):721-36. doi: 10.1002/jqs.1092. PubMed PMID:
1006 WOS:000250415800007.

- 1007 32. Pearce NJG, Eastwood WJ, Westgate JA, Perkins WT. Trace-element composition of
1008 single glass shards in distal Minoan tephra from SW Turkey. *J Geol Soc.* 2002;159:545-
1009 56. doi:10.1144/0016-764901-129. PubMed PMID: WOS:000177855400007.
- 1010 33. Pearce NJG, Westgate JA, Perkins WT, Preece SJ. The application of ICP-MS methods to
1011 tephrochronological problems. *Applied Geochemistry.* 2004;19(3):289-322. doi:
1012 10.1016/S0883-2729(03)00153-7. PubMed PMID: WOS:000189101300003.
- 1013 34. Bertrand S, Castiaux J, Juvigne E. Tephrostratigraphy of the late glacial and Holocene
1014 sediments of Puyehue Lake (Southern Volcanic Zone, Chile, 40 degrees S). *Quaternary*
1015 *Research.* 2008;70(3):343-57. doi: 10.1016/j.yqres.2008.06.001. PubMed PMID:
1016 WOS:000260841600001.
- 1017 35. Cioni R, D'Oriano C, Bertagnini A. Fingerprinting ash deposits of small scale eruptions by
1018 their physical and textural features. *Journal of Volcanology and Geothermal Research.*
1019 2008;177(1):277-87. doi: 10.1016/j.jvolgeores.2008.06.003. PubMed PMID:
1020 WOS:000260986600021.
- 1021 36. Davies SM. Were there two Borrobol Tephra during the early Lateglacial period:
1022 implications for tephrochronology? *Quat Sci Rev.* 2004;23(5-6):581-9. doi:
1023 10.1016/j.quascirev.2003.11.006. PubMed PMID: ISI:000220163100004.
- 1024 37. Davies SM, Abbott PM, Meara RH, Pearce NJG, Austin WEN, Chapman MR, et al. A North
1025 Atlantic tephrostratigraphical framework for 130-60 ka b2k: new tephra discoveries,
1026 marine-based correlations, and future challenges. *Quat Sci Rev.* 2014;106:101-21. doi:
1027 10.1016/j.quascirev.2014.03.024. PubMed PMID: WOS:000348010900008.
- 1028 38. Hillenbrand CD, Moreton SG, Caburlotto A, Pudsey CJ, Lucchi RG, Smellie JL, et al.
1029 Volcanic time-markers for Marine Isotopic Stages 6 and 5 in Southern Ocean sediments
1030 and Antarctic ice cores: implications for tephra correlations between palaeoclimatic
1031 records. *Quat Sci Rev.* 2008;27(5-6):518-40. doi: 10.1016/j.quascirev.2007.11.009.
1032 PubMed PMID: WOS:000255351900007.
- 1033 39. Knott JR, Sarna-Wojcicki AM, Montanez IP, Wan E. Differentiating the Bishop ash bed
1034 and related tephra layers by elemental-based similarity coefficients of volcanic glass
1035 shards using solution inductively coupled plasma-mass spectrometry (S-ICP-MS).
1036 *Quaternary International.* 2007;166:79-86. doi: 10.1016/j.quaint.2006.12.014. PubMed
1037 PMID: WOS:000247166400008.
- 1038 40. Pollard AM, Blockley SPE, Lane CS. Some numerical considerations in the geochemical
1039 analysis of distal microtephra. *Applied Geochemistry.* 2006;21(10):1692-714. doi:
1040 10.1016/j.apgeochem.2006.07.007. PubMed PMID: WOS:000241641000008.
- 1041 41. Tamura I, Yamazaki H, Mizuno K. Characteristics for the recognition of Pliocene and
1042 early Pleistocene marker tephra in central Japan. *Quaternary International.*
1043 2008;178:85-99. doi: 10.1016/j.quaint.2007.04.002. PubMed PMID:
1044 ISI:000255304900009.
- 1045 42. Turney CSM, Blockley SPE, Lowe JJ, Wulf S, Branch NP, Mastrolorenzo G, et al.
1046 Geochemical characterization of Quaternary tephra from the Campanian Province,
1047 Italy. *Quaternary International.* 2008;178:288-305. doi: 10.1016/j.quaint.2007.02.007.
1048 PubMed PMID: WOS:000255304900023.
- 1049 43. Shane P, Martin SB, Smith VC, Beggs KF, Darragh MB, Cole JW, et al. Multiple rhyolite
1050 magmas and basalt injection in the 17.7 ka Rerewhakaaitu eruption episode from
1051 Tarawera volcanic complex, New Zealand. *Journal of Volcanology and Geothermal*
1052 *Research.* 2007;164(1-2):1-26. doi: 10.1016/j.jvolgeores.2007.04.003. PubMed PMID:
1053 WOS:000248766400001.

- 1054 44. Shane P, Nairn IA, Martin SB, Smith VC. Compositional heterogeneity in tephra deposits
 1055 resulting from the eruption of multiple magma bodies: Implications for
 1056 tephrochronology. *Quaternary International*. 2008;178:44-53. doi:
 1057 10.1016/j.quaint.2006.11.014. PubMed PMID: WOS:000255304900006.
- 1058 45. Ruddiman WF, Glover LK. Ice-Rafted Volcanic Ash - a Tracer of North-Atlantic Paleo-
 1059 Circulation. *Transactions-American Geophysical Union*. 1972;53(4):423-&. PubMed
 1060 PMID: WOS:A1972L950100407.
- 1061 46. Ruddiman WF, Glover LK. Vertical Mixing of Ice-Rafted Volcanic Ash in North-Atlantic
 1062 Sediments. *Geological Society of America Bulletin*. 1972;83(9):2817-&. doi: Doi
 1063 10.1130/0016-7606(1972)83[2817:Vmoiva]2.0.Co;2. PubMed PMID:
 1064 WOS:A1972N400300019.
- 1065 47. Pollard AM, Blockley SPE, Ward KR. Chemical alteration of tephra in the depositional
 1066 environment: theoretical stability modelling. *Journal of Quaternary Science*.
 1067 2003;18(5):385-94. doi: 10.1002/jqs.760. PubMed PMID: WOS:000184038700002.
- 1068 48. Blockley SPE, Pyne-O'Donnell SDF, Lowe JJ, Matthews IP, Stone A, Pollard AM, et al. A
 1069 new and less destructive laboratory procedure for the physical separation of distal glass
 1070 tephra shards from sediments. *Quat Sci Rev*. 2005;24(16-17):1952-60. doi:
 1071 10.1016/j.quascirev.2004.12.008. PubMed PMID: WOS:000231044100015.
- 1072 49. Casely AF, Dugmore AJ. Climate change and 'anomalous' glacier fluctuations: the
 1073 southwest outlets of Myrdalsjökull, Iceland. *Boreas*. 2004;33(2):108-22. doi:
 1074 10.1080/03009480410001136. PubMed PMID: WOS:000221110900002.
- 1075 50. Dugmore AJ, Church MJ, Mairs KA, McGovern TH, Perdikaris S, Vesteinsson O.
 1076 Abandoned farms, volcanic impacts, and woodland management: Revisiting
 1077 pjorsardalur, the "Pompeii of iceland". *Arctic Anthropology*. 2007;44(1):1-11. PubMed
 1078 PMID: WOS:000248704400001.
- 1079 51. Dugmore AJ, Sugden DE. Do the anomalous fluctuations of Solheimajökull reflect ice-
 1080 divide migration. *Boreas*. 1991;20:105-13.
- 1081 52. Edwards KJ, Dugmore AJ, Blackford JJ. Vegetational response to tephra deposition and
 1082 land-use change in Iceland: a modern analogue and multiple working hypothesis
 1083 approach to tephropalynology. *Polar Record*. 2004;40(213):113-20.
 1084 doi:10.1017/S0032247403003000. PubMed PMID: WOS:000226634700003.
- 1085 53. Hafliðason H, Eiriksson J, Van Kreveld S. The tephrochronology of Iceland and the North
 1086 Atlantic region during the Middle and Late Quaternary: a review. *Journal of Quaternary
 1087 Science*. 2000;15(1):3-22. PubMed PMID: ISI:000085226600002.
- 1088 54. Hallsdóttir M. Pollen analytical studies of human influence on vegetation in relation to
 1089 the Landnám tephra layer in southwest Iceland 1987. 45 p.
- 1090 55. Kirkbride MP, Dugmore AJ. Timing and significance of mid-Holocene glacier advances in
 1091 northern and central Iceland. *Journal of Quaternary Science*. 2001;16(2):145-53.
 1092 doi:10.1002/jqs.589. PubMed PMID: WOS:000167761700005.
- 1093 56. Kirkbride MP, Dugmore AJ. Glaciological response to distal tephra fallout from the 1947
 1094 eruption of Hekla, south Iceland. *Journal of Glaciology*. 2003;49(166):420-8.
 1095 doi:10.3189/172756503781830575. PubMed PMID: WOS:000220521200011.
- 1096 57. Kirkbride MP, Dugmore AJ. Responses of mountain lee caps in central Iceland to
 1097 Holocene climate change. *Quat Sci Rev*. 2006;25(13-14):1692-707. doi:
 1098 10.1016/j.quascirev.2005.12.004. PubMed PMID: WOS:000239940000019.

- 1099 58. Larsen G, editor Holocene volcanism in Iceland and tephrochronology as a tool in
1100 volcanology. Iceland 2000 – Modern Processes and Past Environments; 2000 April 27th-
1101 29th, 2000; Keele University, UK.
- 1102 59. Lawson IT, Gathorne-Hardy FJ, Church MJ, Newton AJ, Edwards KJ, Dugmore AJ, et al.
1103 Environmental impacts of the Norse settlement: palaeoenvironmental data from
1104 Myvatnssveit, northern Iceland. *Boreas*. 2007;36(1):1-19. doi:
1105 10.1080/0300948060082798. PubMed PMID: WOS:000244148600001.
- 1106 60. Larsen C, Newton AJ, Dugmore AJ, Vilmundardottir EG. Geochemistry, dispersal,
1107 volumes and chronology of Holocene from the Katla volcanic silicic tephra layers
1108 system, Iceland. *Journal of Quaternary Science*. 2001;16(2):119-32. PubMed PMID:
1109 WOS:000167761700003.
- 1110 61. Wastegard S. Early to middle Holocene silicic tephra horizons from the Katla volcanic
1111 system, Iceland: new results from the Faroe Islands. *Journal of Quaternary Science*.
1112 2002;17(8):723-30. doi: 10.1002/jqs.724. PubMed PMID: WOS:000180149700001.
- 1113 62. Selbekk RS, Tronnes RG. The 1362 AD Oraefajoull eruption, Iceland: Petrology and
1114 geochemistry of large-volume homogeneous rhyolite. *Journal of Volcanology and*
1115 *Geothermal Research*. 2007;160(1-2):42-58. doi: 10.1016/j.jvolgeores.2006.08.005.
1116 PubMed PMID: WOS:000244215100003.
- 1117 63. Sarna-Wojcicki A. Tephrochronology. In: Stratton-Noller J, Sowers, J. M., Lettis, W. R.,
1118 editor. *Quaternary Geochronology: Methods and Applications 2000*.
- 1119 64. Shane P. Tephrochronology: a new Zealand case study. *Earth-Science Reviews*.
1120 2000;49(1-4):223-59. doi:10.1016/S0012-8252(99)00058-6. PubMed PMID:
1121 WOS:000086702100005.
- 1122 65. Aitken M.J., 1985, *Thermoluminescence Dating*, Academic Press
- 1123 66. Sanderson D.C.W., 1982, *The thermoluminescence of archaeological glass*, MPhil
1124 Thesis, University of Bradford)
- 1125 67. Ward S. The thermoluminescence of glass slices and their potential as radiation
1126 dosimeters in the 0-160 kGy range. BSc dissertation, University of Strathclyde; 1988.
- 1127 68. Huntley DJ, Bailey DC. Obsidian Source identification by thermoluminescence.
1128 *Archaeometry*. 1978;20(2):159-70.
- 1129 69. Westgate JA. Isothermal Plateau Fission-Track Ages of Hydrated Glass Shards from Silicic
1130 Tephra Beds. *Earth and Planetary Science Letters*. 1989;95(3-4):226-34.
1131 doi:10.1016/0012-821x(89)90099-X. PubMed PMID: WOS:A1989CC77700004.
- 1132 70. Westgate J, Sandhu A, Shane P. Fission-Track Dating. In: Taylor RE, Aitken MJ, editors.
1133 *Chronometric Dating in Archaeology*. Boston, MA: Springer US; 1997. p. 127-58.
- 1134 71. Westgate JA, Preece SJ, Froese DG, Walter RC, Sandhu AS, Schweger CE. Dating early
1135 and middle (Reid) pleistocene glaciations in central Yukon by tephrochronology.
1136 *Quaternary Research*. 2001;56(3):335-48. doi:10.1006/qres.2001.2274. PubMed PMID:
1137 WOS:000172212000005.
- 1138 72. Bigazzi G, Laurenzi MA, Soligo M, Tuccimei P. Multi-method approach to dating glass:
1139 The case of Basiluzzo Islet (Aeolian archipelago, Italy). *Journal of Volcanology and*
1140 *Geothermal Research*. 2008;177(1):244-50. doi: 10.1016/j.jvolgeores.2007.10.005.
1141 PubMed PMID: WOS:000260986600018.
- 1142 73. Berger GW. The Use of Glass for Dating Volcanic Ash by Thermoluminescence. *Journal*
1143 *of Geophysical Research-Solid Earth*. 1991;96(B12):19705-20. doi: 10.1029/91jb01899.
1144 PubMed PMID: WOS:A1991GQ69100013.

- 1145 74. Berger GW. Dating Volcanic Ash by Use of Thermoluminescence. *Geology*.
 1146 1992;20(1):11-4. doi:10.1130/0091-7613(1992)020<0011:Dvabuo>2.3.Co;2. PubMed
 1147 PMID: WOS:A1992GZ53700003.
- 1148 75 Roberts SJ, Sigurvinsson JR, Westgate JA, Sandhu A. Late Pliocene glaciation and
 1149 landscape evolution of Vestfirðir, Northwest Iceland. *Quat Sci Rev*. 2007;26(1-2):243-
 1150 63. doi: 10.1016/j.quascirev.2006.09.004. PubMed PMID: ISI:000244024800017.
- 1151 76. Jorgensen KA. The Thorsmork Ignimbrite - an Unusual Comenditic Pyroclastic Flow in
 1152 Southern Iceland. *Journal of Volcanology and Geothermal Research*. 1980;8(1):7-22.
 1153 doi:10.1016/0377-0273(80)90004-9. PubMed PMID: WOS:A1980KF92900002.
- 1154 77. Jorgensen KA. The eruption of Þórsmörk Ignimbrite, south Iceland. Reykjavik: Nordic
 1155 Volcanological Institute, Report no. 8103., 1981.
- 1156 78. McGarvie DW, editor Torfajökull – the world’s most active rhyolite volcano. Iceland
 1157 2000 – Modern Processes and Past Environments; 2000 April 27th-29th 2000; Keele
 1158 University, UK.
- 1159 79. Thórarinsson S, Sæmundsson K. Volcanic activity in historical time. *Jökull*. 1979;29:29-
 1160 32.
- 1161 80. Jakobsson SP. Outline of the petrology of Iceland. *Jökull*. 1979;29:57-73.
- 1162 81. Jakobsson SP. Chemistry and distribution pattern of Recent basaltic rocks in Iceland.
 1163 *Lithos*. 1972;5:365-86.
- 1164 82. Imsland P. The Petrology of Iceland: Some General Remarks. Reykjavik: Nordic
 1165 Volcanological Institute Report 7808, pp. 2, 1978.
- 1166 83. Sæmundsson K. Outline of the Geology of Iceland. *Jökull*. 1979;29:7-28.
- 1167 84. Jorgensen KA. Mineralogy and Petrology of Alkaline Granophyric Xenoliths from the
 1168 Thorsmork Ignimbrite, Southern Iceland. *Lithos*. 1987;20(2):153-68. doi: Doi
 1169 10.1016/0024-4937(87)90004-1. PubMed PMID: WOS:A1987G439900004.
- 1170 85. Sparks RSJ, Bursik MI, Carey SN, Gilbert JS, Glaze LS, Sigurdsson H, et al. *Volcanic Plumes*.
 1171 Chichester: John Wiley and Sons; 1997. 574 p.
- 1172 86. Ram M, Gayley RI. Long-Range Transport of Volcanic Ash to the Greenland Ice-Sheet.
 1173 *Nature*. 1991;349(6308):401-4. doi:10.1038/349401a0. PubMed PMID:
 1174 WOS:A1991EV51400045.
- 1175 87. Ram M, Donarummo J, Sheridan M. Volcanic ash from Icelandic similar to 57,300 yr BP
 1176 eruption found in GISP2 (Greenland) ice core. *Geophysical Research Letters*.
 1177 1996;23(22):3167-9. doi:10.1029/96gl03099. PubMed PMID: WOS:A1996VQ92400025.
- 1178 88. Hafliðason H, Eiríksson J, Van Kreveld S. The tephrochronology of Iceland and the North
 1179 Atlantic region during the Middle and Late Quaternary: a review. *Journal of Quaternary
 1180 Science*. 2000;15(1):3-22. PubMed PMID: ISI:000085226600002.
- 1181 89. Sparks RSJ, Wilson L, Sigurdsson H. The Pyroclastic Deposits of the 1875 Eruption of
 1182 Askja, Iceland. *Philos T R Soc A*. 1981;299(1447):241-+. doi:10.1098/rsta.1981.0023.
 1183 PubMed PMID: WOS:A1981LA47100001.
- 1184 90. Sigurdsson H, Sparks RSJ. Petrology of Rhyolitic and Mixed Magma Ejecta from the 1875
 1185 Eruption of Askja, Iceland. *Journal of Petrology*. 1981;22(1):41-84. PubMed PMID:
 1186 WOS:A1981LD62800002.
- 1187 91. Macdonald R, Sparks RSJ, Sigurdsson H, Matthey DP, Mcgarvie DW, Smith RL. The 1875
 1188 Eruption of Askja Volcano, Iceland - Combined Fractional Crystallization and Selective
 1189 Contamination in the Generation of Rhyolitic Magma. *Mineralogical Magazine*.
 1190 1987;51(360):183-202. doi:10.1180/minmag.1987.051.360.01. PubMed PMID:
 1191 WOS:A1987H622300001.

- 1192 92. Mohn H. Askeregnen den 29de-30te Marts 1875. Forhandlinger i Videnskaps-selskabet
1193 i Christiania aar 1877. 1877;10: 1–12.
- 1194 93. Einarsson T. Tephrochronology. In: Berglund BE, editor. Handbook of Holocene
1195 Palaeoecology and Palaeohydrology: John Wiley and Sons; 1986. p. 329-42.
- 1196 94. Bergman J, Wastegard S, Hammarlund D, Wohlfarth B, Roberts SJ. Holocene tephra
1197 horizons at Klocka Bog, west-central Sweden: aspects of reproducibility in subarctic peat
1198 deposits. *Journal of Quaternary Science*. 2004;19(3):241-9. doi: 10.1002/jqs.833.
1199 PubMed PMID: WOS:000221238800003.
- 1200 95. Pilcher JR, Hall VA, McCormac FG. Dates of Holocene Icelandic Volcanic-Eruptions from
1201 Tephra Layers in Irish Peats. *Holocene*. 1995;5(1):103-10.
1202 doi:10.1177/095968369500500111. PubMed PMID: WOS:A1995QX87900011.
- 1203 96. Thórarinnsson S. The Öraefajökull eruption of 1362. *Acta Naturalia Islandica*. 1958;2(2):1-
1204 99.
- 1205 97. Sigurvinsson JR. Weichselian glacial lake deposits in the Highlands of north-western
1206 Iceland. *Jökull*. 1983;33:99-109.
- 1207 98. McKeever SWS. Thermoluminescence of solids. Cambridge: Cambridge University Press;
1208 1985. 312 p.
- 1209 99. Wintle AG. Luminescence dating: Laboratory procedures and protocols. *Radiation*
1210 *Measurements*. 1997;27(5-6):769-817. doi:10.1016/S1350-4487(97)00220-5. PubMed
1211 PMID: WOS:000072413000007.
- 1212 100. Aitken MJ. An introduction to optical dating. *The Dating of Quaternary Sediments by*
1213 *the Use of Photon-stimulated Luminescence*. Oxford: Oxford University Press; 1998. 270
1214 p.
- 1215 101. Zander A, Duller GAT, Wintle AG. Multiple and single aliquot luminescence dating
1216 techniques applied to quartz extracted from Middle and Upper Weichselian loess,
1217 Zemechy, Czech Republic. *Journal of Quaternary Science*. 2000;15(1):51-60.
1218 doi:10.1002/(Sici)1099-1417(200001)15:1<51::Aid-Jqs468>3.0.Co;2-6. PubMed PMID:
1219 WOS:000085226600005.
- 1220 102. Turney CSM, Harkness DD, Lowe JJ. The use of microtephra horizons to correlate Late-
1221 glacial lake sediment successions in Scotland. *Journal of Quaternary Science*.
1222 1997;12(6):525-31. doi:10.1002/(Sici)1099-1417(199711/12)12:6<525::Aid-
1223 Jqs347>3.3.Co;2-D. PubMed PMID: WOS:000071733500007.
- 1224 103. Murray AS, Wintle AG. Luminescence dating of quartz using an improved single-aliquot
1225 regenerative-dose protocol. *Radiation Measurements*. 2000;32(1):57-73. doi:
1226 10.1016/S1350-4487(99)00253-X. PubMed PMID: WOS:000084790600008.
- 1227 104. Murray AS, Wintle AG. The single aliquot regenerative dose protocol: potential for
1228 improvements in reliability. *Radiation Measurements*. 2003;37(4-5):377-81. doi:
1229 10.1016/S1350-4487(03)00053-2. PubMed PMID: WOS:000184110400015.
- 1230 105. Pawley SM, Bailey RM, Rose J, Moorlock BSP, Hamblin RJO, Booth SJ, et al. Age limits on
1231 Middle Pleistocene glacial sediments from OSL dating, north Norfolk, UK. *Quat Sci Rev*.
1232 2008;27(13-14):1363-77. doi: 10.1016/j.quascirev.2008.02.013. PubMed PMID:
1233 WOS:000257604000006.
- 1234 106. Zimmerman DW. Thermoluminescent Dating Using Fine Grains from Pottery.
1235 *Archaeometry*. 1971;13(Feb):29-52. doi: DOI 10.1111/j.1475-4754.1971.tb00028.x.
1236 PubMed PMID: WOS:A1971Y040400005.
- 1237 107. Bell WT. Alpha dose attenuation in quartz grains for thermoluminescence dating.
1238 *Ancient TL*. 1980;12:4-8.

- 1239 108. Mejdahl V. Thermoluminescence Dating - Beta-Dose Attenuation in Quartz Grains.
 1240 Archaeometry. 1979;21(Feb):61-72. doi: DOI 10.1111/j.1475-4754.1979.tb00241.x.
 1241 PubMed PMID: WOS:A1979GM02300005.
- 1242 109. Nambi KSV, Aitken MJ. Annual Dose Conversion Factors for TL-and-ESR Dating.
 1243 Archaeometry. 1986;28:202-5. doi10.1111/j.1475-4754.1986.tb00388.x. PubMed
 1244 PMID: WOS:A1986D630100007.
- 1245 110. Wintle AG. Detailed Study of a Thermoluminescent Mineral Exhibiting Anomalous
 1246 Fading. Journal of Luminescence. 1977;15(4):385-93. doi:10.1016/0022-
 1247 2313(77)90037-0. PubMed PMID: WOS:A1977EB75500002.
- 1248 111. Sanderson DCW. Thermoluminescence dating of Scottish vitrified forts: Paisley College
 1249 of Technology; 1986 uk.bl.ethos.376105
- 1250 112. Toyoda S, Tsukamoto S, Hameau S, Usui H, Suzuki T. Dating of Japanese Quaternary
 1251 tephra by ESR and luminescence methods. Quaternary Geochronology. 2006;1(4):320-
 1252 6. doi: 10.1016/j.quageo.2006.03.007. PubMed PMID: WOS:000247209900010.
- 1253 113. Auclair M, Lamothe M, Lagroix F, Banerjee SK. Luminescence investigation of loess and
 1254 tephra from halfway house section, central Alaska. Quaternary Geochronology.
 1255 2007;2(1-4):34-8. doi: 10.1016/j.quageo.2006.05.009. PubMed PMID:
 1256 WOS:000247210000008.
- 1257 114. Tsukamoto S, Murray AS, Huot S, Watanuki T, Denby PM, Botter-Jensen L.
 1258 Luminescence property of volcanic quartz and the use of red isothermal TL for dating
 1259 tephra. Radiation Measurements. 2007;42(2):190-7. doi:
 1260 10.1016/j.radmeas.2006.07.008. PubMed PMID: WOS:000247516300010.
 1261
- 1262 115. Tsukamoto S. Luminescence, Volcanic Rocks. In: Rink JW, Thompson J, editors.
 1263 Encyclopedia of Scientific Dating Methods. Dordrecht: Springer Netherlands; 2013. p. 1-
 1264 5.
- 1265 116. Sanderson DCW. Fading of Thermo-Luminescence in Feldspars - Characteristics and
 1266 Corrections. Nuclear Tracks and Radiation Measurements. 1988;14(1-2):155-61.
 1267 PubMed PMID: WOS:A1988P853300023.
- 1268 117. Visocekas R. La luminescence de la calcite après irradiation cathodique:
 1269 thermoluminescence et luminescence par effet tunnel. France: Université de Pierre et
 1270 Marie Curie; 1979.
- 1271 118. Lamothe M, Auclair M. A solution to anomalous fading and age shortfalls in optical
 1272 dating of feldspar minerals. Earth and Planetary Science Letters. 1999;171(3):319-23.
 1273 doi: 10.1016/S0012-821x(99)00180-6. PubMed PMID: WOS:000082374200001.
- 1274 119. Templer RH. The Localised Transition Model of Anomalous Fading. 1986. p. 493-7.
- 1275 120. Morthekai P, Jain M, Murray AS, Thomsen KJ, Botter-Jensen L. Fading characteristics of
 1276 martian analogue materials and the applicability of a correction procedure. Radiation
 1277 Measurements. 2008;43(2-6):672-8. doi: 10.1016/j.radmeas.2008.02.019. PubMed
 1278 PMID: WOS:000257808000117.
- 1279 121. Chawla S, Rao TKG, Singhvi AK. Quartz thermoluminescence: Dose and dose-rate effects
 1280 and their implications. Radiation Measurements. 1998;29(1):53-63. doi:
 1281 10.1016/S1350-4487(97)00200-X. PubMed PMID: WOS:000072761500007.
- 1282 122. Bell WT. Attenuation factors for the absorbed radiation dose in quartz grains for
 1283 luminescence dating. Ancient TL. 1979;8:2-13.
- 1284 123. Bell WT. TL dating: radiation dose rate data. Archaeometry. 1979;21:243.

- 1285 124. Horn P, Müller-Sohnius D, Storzer D, Zöller L. K-Ar-, fission-track-, and thermolumines-
1286 cence ages of Quaternary volcanic tuffs and their bearing on Acheulian artifacts from
1287 Bori, Kukdi Valley, Pune District, India. *Zeitschrift der Deutschen geologischen*
1288 *Gesellschaft*. 1993;144:326-9.
- 1289 125. Wolfe CJ, Bjarnason IT, VanDecar JC, Solomon SC. Seismic structure of the Iceland
1290 mantle plume. *Nature*. 1997;385(6613):245-7. doi:10.1038/385245a0. PubMed PMID:
1291 WOS:A1997WC71100044.
- 1292 126. LeMaitre RW, Bateman P, Dudek A, Keller J, Lameyre Le Bas MJ, Sabine PA, et al. A
1293 classification of igneous rocks and glossary of terms. Oxford: Blackwell; 1989.
- 1294 127. Rickwood PC. Boundary Lines within Petrologic Diagrams Which Use Oxides of Major
1295 and Minor Elements. *Lithos*. 1989;22(4):247-63. doi:10.1016/0024-4937(89)90028-5.
1296 PubMed PMID: WOS:A1989U514400001.
- 1297 128. Oskarsson N, Steinthorsson S, Sigvaldason GE. Iceland Geochemical Anomaly - Origin,
1298 Volcanotectonics, Chemical Fractionation and Isotope Evolution of the Crust. *J Geophys*
1299 *Res-Solid*. 1985;90(Nb12):11-25. doi:10.1029/JB090iB12p10011. PubMed PMID:
1300 WOS:A1985ASE4800005.
- 1301 129. Sweatman TR, Long JVP. Quantitative electron microprobe analysis of rock forming
1302 minerals. *Journal of Petrology*. 1969;7:332-79.
- 1303 130. Prescott JR, Hutton JT. Cosmic ray contributions to dose rates for luminescence and ESR
1304 dating: large depths and long-term time variations. *Radiation Measurements*.
1305 1994;23(497-500).
- 1306 131. Norrish K, Hutton JT. An accurate X-ray spectrographic method for the analysis of a wide
1307 range of geological samples. *Geochimica et Cosmochimica Acta*. 1969;33:431-53.
- 1308 132. Aitken MJ, Bowman SGE. Thermoluminescence dating: assessment of alpha particle
1309 contribution. *Archaeometry*. 1975;17:132-8.
- 1310 133. Berger GW. Progress in luminescence dating methods for Quaternary sediments. In:
1311 Rutter NW, Catto NR, editors. *Dating Methods for Quaternary Deposits: Geological*
1312 *Association of Canada*; 1995. p. 81-104.
- 1313